Heliyon 5 (2019) e02359

Contents lists available at ScienceDirect

Heliyon

journal homepage: www.heliyon.com

Polyurethane-carbon microfiber composite coating for electrical heating of concrete pavement surfaces

Alireza Sassani [a,*], Ali Arabzadeh [a], Halil Ceylan [b], Sunghwan Kim [c], Kasthurirangan Gopalakrishnan [d,e], Peter C. Taylor [f], Ali Nahvi [a]

[a] 176 Town Engineering Building, Department of Civil, Construction, and Environmental Engineering, Iowa State University, Ames, IA 50011, USA
[b] Program for Sustainable Pavement Engineering and Research (PROSPER), 406 Town Engineering Building, Department of Civil, Construction, and Environmental Engineering, Iowa State University, Ames, IA 50011-3232, USA
[c] 24 Town Engineering Building, Department of Civil, Construction, and Environmental Engineering, Iowa State University, Ames, IA 50011-3232, USA
[d] 354 Town Engineering Building, Department of Civil, Construction, and Environmental Engineering, Iowa State University, Ames, IA 50011-3232, USA
[e] SRM University, AP, Amaravati 522 502, India
[f] National Concrete Pavement Technology Center, 2711 South Loop Drive, Suite 4700, Iowa State University, Ames, IA 50011-8664, USA

ARTICLE INFO

Keywords:
Civil engineering
Mechanical engineering
Materials science
Composite
Portland cement concrete
Electrically conductive coating
Polyurethane
Heated pavement systems
Carbon fiber

ABSTRACT

Electrically-heated pavements have attracted attention as alternatives to the traditional ice/snow removal practices. Electrically conductive polymer-carbon composite coatings provide promising properties for this application. Based on the concept of joule heating, the conductive composite can be utilized as a resistor that generates heat by electric current and increases the surface temperature to melt the ice and snow on the pavement surface. This research investigates the feasibility of applying an electrically conductive composite coating made with a Polyurethane (PU) binder and micrometer-scale carbon fiber (CMF) filler as the electrical heating materials on the surface of Portland cement concrete (PCC) pavements. PU-CMF composite coatings were prepared using different volume fractions of CMF, applied on the PCC surfaces, and evaluated in terms of volume conductivity, resistive heating ability, durability, and surface friction properties at the proof-of-concept level. A conceptual cost analysis was performed to compare this method with other heated pavement systems with respect to economic viability. Percolative behavior of CMF in PU matrix was captured and most desirable CMF dosage rates in terms of each performance parameter were investigated. Two percolation transition zones were identified for CMF in PU matrix at dosage rate ranges of 0.25–1% and 4–10%. The composites exhibited their most desirable performance and properties at CMF dosage rates greater than 10% and smaller than 15%.

1. Introduction

Keeping the surface of paved areas free of ice and snow is a major challenge during harsh winter conditions. Traditional methods of ice/snow removal from pavements that use deicing chemicals and mechanical removal are associated with large manpower, sophisticated machinery, environmentally harmful chemicals, damage to pavements, and inadequate effectiveness in extreme weather conditions [1, 2, 3, 4, 5, 6, 7, 8]. Most deicing chemicals are not effective at temperatures below -9 °C [9, 10]. Only calcium chloride-based deicers that increase risk of early distress for concrete pavements can be used at temperatures colder than -17 °C (1.4°F) [7]. Application of deicing chemicals is especially associated with negative environmental impacts [11, 12, 13, 14, 15, 16, 17, 18, 19, 20]. In recent years, alternative methods have been proposed and tested for removing ice and snow from paved surfaces; among them are thermal modification of pavement materials [21], application of superhydrophobic coatings on pavement surfaces [22, 23, 24, 25] and electrically heated pavement systems [4, 26, 28, 29, 30, 31, 32, 33, 34, 35, 36, 37, 38, 39, 40, 41, 42, 43, 44, 45]. Electrically heated pavement systems have gained recent attention as an alternative to traditional methods to overcome winter pavement maintenance problems [28, 46]. Two approaches to electrical heating of pavements have so far been adopted in the literature: (a) embedding electrically heating sheet/grille elements inside the pavement [4, 26], and (b) application of electrically conductive concrete/asphalt pavements [27, 28, 29, 30, 31, 32, 33, 34, 35, 36, 37, 38, 39, 40, 41, 42, 43]. Application of electrically conductive

* Corresponding author.
E-mail address: asassani@iastate.edu (A. Sassani).

https://doi.org/10.1016/j.heliyon.2019.e02359
Received 30 October 2018; Received in revised form 3 July 2019; Accepted 20 August 2019

coating in heated pavements is a new and, to the best of authors' knowledge, unprecedented method for producing electrically heated pavements.

Various types of polymers have been used for modifying pavement materials, mostly in the form of an additive to asphalt-based concretes [47, 48, 49, 50, 51]. Numerous studies have investigated the feasibility and benefits of the application of different polymer-based and Portland cement-based coating on concrete substrates. Water-repellent and water-proofing coatings on Portland cement concrete (PCC) and asphalt concrete materials have been extensively studied [2, 22, 23, 25, 52, 53, 54, 55, 56, 57]. On the contrary, there is very limited information regarding electrically conductive coating on concrete surfaces. The only application of electrically conductive coatings on concrete surfaces, in the relevant literature, involve using epoxy resin-based [58] or Portland cement-based [59, 60] coatings as the anode in corrosion protection and/or chloride extraction practices. However, electrically conductive composites are an important group of versatile materials with various engineering applications [61]. Electrically conductive coatings and thin films have been developed, mainly for application in circuitry [62], production of conductive papers [63, 64], electromagnetic interference shielding [65, 66, 67], and sensor systems [68, 69, 70, 71]. In addition, Elsharkawy et al. [48] produced water-repellent and electrically-heated coatings for metallic surfaces using carbon nanofibers dispersed in fluoroacrylic copolymer matrix.

The electrically conductive thin films and coatings are, typically, produced through dispersing a filler material such as carbon black [72], carbon nanotubes/nanofibers [65, 67, 73], or graphene [63, 74], in a polymer matrix and casting the mixture on the substrate [72]. Different polymers can be used as binder phase in coatings. Epoxy resin has been used as a binder material on various surfaces such as PCC [2, 24], asphalt cement concrete [22, 23, 25], and glass [75] to bind the nano-particles and adhere to the substrate. Fluorinated polymers such as Poly (vinylidene fluoride) (PVDF) have been used in superhydrophobic coatings as a matrix [67, 76, 77, 78]. Tiwari et al. [76] and Das et al. [67] fabricated large-area sprayable superhydrophobic coatings with PVDF as binder. However, because of low strength and weak binding ability of PVDF, it needs to be used in conjunction with other binders. Poly (ethyl 2-cyanoacrylate) (PECA) and Poly (methyl methacrylate) (PMMA or acrylic resin) are commonly used as the additional binder materials with PVDF or used alone as the binder phase [67, 76, 79, 80]. A group of polymers gaining increasing attention in the field of coating materials are Polyurethane (PU) compounds, a wide variety of materials that provide superior binding and adhesion properties. Polyurethane elastomers are thermally stable [81], compatible with carbonaceous materials which are a major component of electrically conductive composites [82, 83, 84, 85], require no or minimal amount of volatile organic solvents [72, 86], and provide high adhesion and durability [87] on most substrates including concrete [88].

Carbonaceous materials, especially carbon fibers [89, 90, 91, 92], carbon nanotubes/nanofibers [93, 94, 95, 96, 97], and graphite powders [60, 98] have been extensively utilized in construction materials. Using nano-size materials in electrically conductive coatings for pavement applications is challenging, particularly because of high cost [90] and hazardous nature [99] of nanoparticles. Gong et al. [100] used carbon felt made of micrometer-size carbon fibers in an electrically conductive polymer composite. Ameli et al. [101] studied the feasibility of polyurethane-carbon fiber composite foam for electromagnetic interference shielding, using carbon fibers with micrometer diameter and millimeter length. In this paper, the term carbon microfiber (CMF) is used to refer to carbon fibers with both diameter and length in micrometer scale. CMF materials are orders of magnitude less expensive than nano-materials, do not pose health hazards, and are easier to disperse in a given matrix (e.g. polymers or cement paste). However, the literature related to the application of such materials in coating mixtures is scarce and, to the best of authors' knowledge, there is no previous report on using PU-CMF composites for electrical heating (a.k.a. resistive heating or joule heating). On the other hand, there is no previous report of PU-CMF composite coating application on concrete structures and pavements.

Previous studies on cost analysis and economics on various types of heated pavement systems - such as hydronic heated pavements, geothermal heated pavement systems; and electrical conductive Portland cement concrete systems (ECON HPS) – showed the gigantic impact of the construction cost of these systems on the total benefit cost ratio [102, 103, 104]. In addition, according to the cost-benefit analysis bulletin published by the Federal Highway Administration (FHWA), construction cost constitutes a big portion of the life cycle cost of the infrastructures. Therefore, to provide some insights in the material and construction costs of heated pavement system made of conductive coatings juxtaposed with other heated pavement systems would be helpful for future economic investigations.

This research investigates the feasibility of using PU-CMF composite coating, made with polyurethane elastomer as binder and milled carbon fiber with micrometer diameter and length as conductive filler, for electrical heating (resistive or joule heating) of PCC pavement surfaces. The required and/or optimum dosage rate of CMF to achieve desirable volume conductivity was determined based on the concept of percolation threshold. Heating capability of the composite coating was studied by active infrared thermography (IRT) in temperature-controlled conditions. The durability of the coating materials under cyclic wheel load and the effect of the coating on skid resistance of Portland cement concrete pavement surfaces were investigated. An initial cost analysis based on the production cost of materials was performed to provide an insight into economic feasibility of this system. The desirable CMF dosage rates with respect to each of the three performance parameters –i.e. volume conductivity, joule heating, and durability-were investigated and reported.

2. Methodology

2.1. Experimental

The CMF used in this study was milled carbon fiber with 7.2 μm nominal diameter, 100 μm nominal length, specific gravity of 1.75, carbon content of 99%, and dry-condition electrical resistivity (volume resistivity) of 1.4×10^{-3} Ω-cm. A one-component fast-drying thermoplastic polyurethane (PU) (by Minwax®) with a kinematic viscosity (at 40 °C) smaller than 2.05×10^{-1} cm^2/s (<20.5 cSt), specific gravity of 0.86, and boiling point of 148 °C was used as the polymer component. The methods proposed in the literature to enhance the dispersion of carbon fibers in cementitious matrices are based on improving the wettability of the fibers [105], therefore, they are not useful in polymer-fiber composites which do not have water or other solvents, as is the case in this study. To improve the dispersion of fibers, the treatment method developed by Xiong et al. [106] for dispersing carbon nanotubes in polyurethane matrix was adopted with some modifications. The as-received CMF was first heat-treated for 4 h at 400 °C while gently blown with air flow. Then, the CMF was dispersed in a 3:1 mixture of sulfuric acid and nitric acid by sonication for 10 min in a bath sonicator at 80 °C. The suspension was then poured on grade 3 filter paper (6 μm pore size), drained off the acid solution, and gently washed with deionized water until the pH of the filtered fluid became close to the pH of the deionized water. Finally, the fibers were collected off the filter paper and desiccated in a vacuum desiccator for 72 h. It should be mentioned that the effect of fiber treatment on the surface chemistry (and dispersion) of CMF is likely different than carbon nanotubes, because the properties of materials in nano-scale tend to differ from their macro- and micro-scale characteristics. However, previous studies have shown adequate effectiveness of such methods in improving the dispersion of carbon fibers with micrometer-scale diameters and millimeter-scale length [105].

The PU-CMF composite suspension was prepared without incorporation of any solvents in the mixture. Because this composite coating is intended for application on pavement surfaces, this approach was

Table 1
Proportions of PU-CMF composite mixtures for determination of percolation transition zone.

CMF dosage rate (% Vol.)	CMF content (g)	PU content (g)
0.25	0.15	30.02
0.50	0.31	29.95
0.75	0.46	29.87
1.00	0.61	29.80
1.50	0.92	29.65
2.00	1.23	29.50
2.50	1.53	29.35
3.00	1.84	29.20
3.50	2.14	29.05
4.00	2.45	28.90
5.00	3.06	28.60
6.00	3.68	28.29
7.50	4.59	27.84
10.00	6.13	27.09
12.50	7.66	26.34
15.00	9.19	25.59
17.50	10.72	24.83
20.00	12.25	24.08

adopted to increase the setting rate of the composite, eliminate the time needed for evaporation of the solvent phase, and thus shorten the closing time of the paved facility. In the absence of solvents, and because of thermo-stability of polyurethanes [81], it was possible to prepare the PU-CMF composite at high temperatures that are above the boiling point of the PU and lower than its degradation temperatures. Thermal degradation of thermoplastic PU takes place above 200 °C [86]. Reduction of the viscosity of PU at higher temperatures [107, 108] facilitates the dispersion of CMF in the PU matrix. The treated CMF were added to the PU component of the composite and the mixture was magnetically stirred at 360 rpm speed and 150 °C temperature for 3 min. Then, the mixture was placed in bath sonicator at 80 °C and sonicated for 10 min, followed by another 3 min of magnetic stirring at the aforementioned speed and temperature. Once the PU-CMF mixture was prepared, it was applied on the specimen surfaces using a brush. The weight of the coating material applied on each specimen was determined by measuring weights of the mixture, the brush, and the specimen before and after coating application.

Percolation is a useful tool for explaining the electrical behavior and determining optimum or required dosage rate of the conductive filler in the composite coatings which consist of an electrically insulating matrix

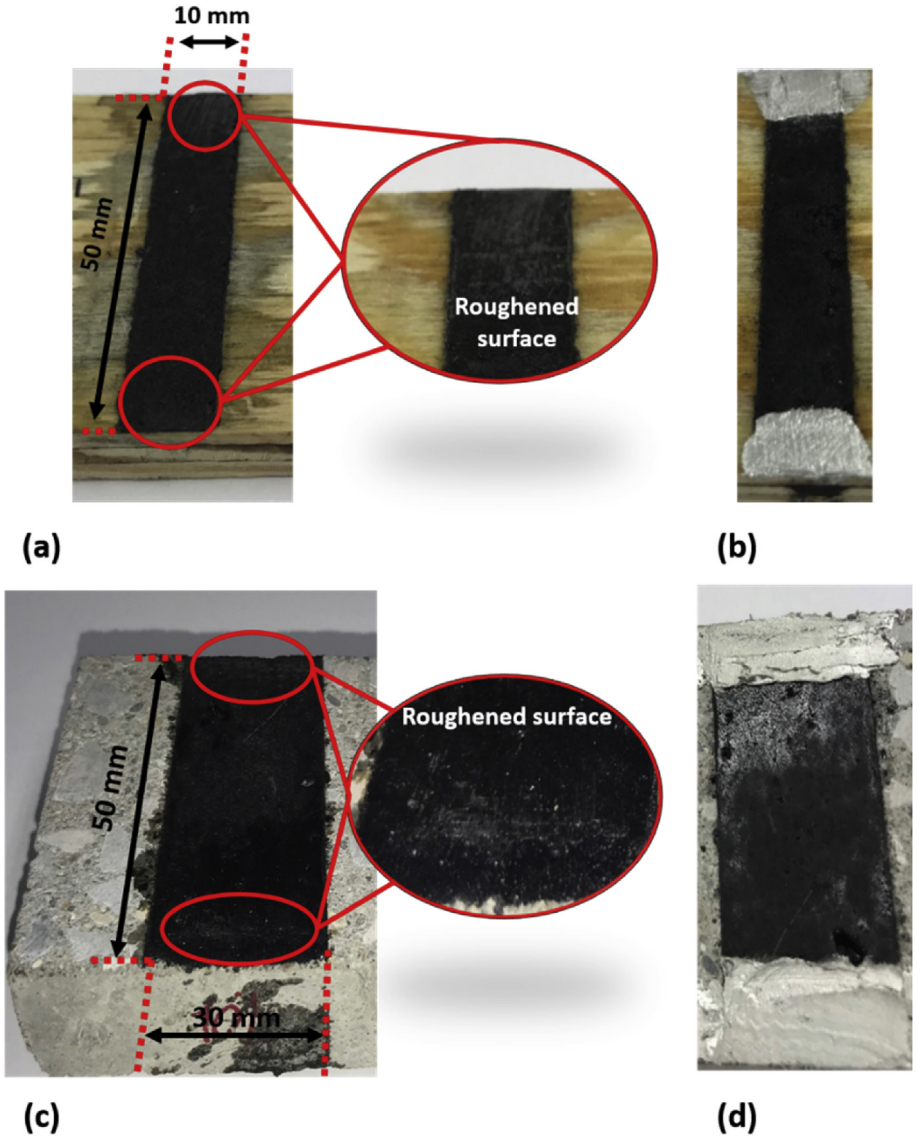

Fig. 1. Specimens for determination of percolation threshold: (a) coating on wood substrate before application of silver paste; (b) coating on wood substrate with silver paste electrode; (c) coating on concrete substrate before application of silver paste; and (d) coating on concrete substrate with silver paste electrode.

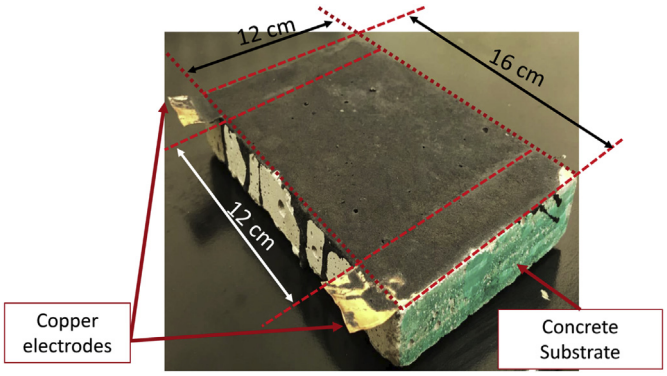

Fig. 2. Concrete specimens coated with PU-CMF composite for resistive heating test.

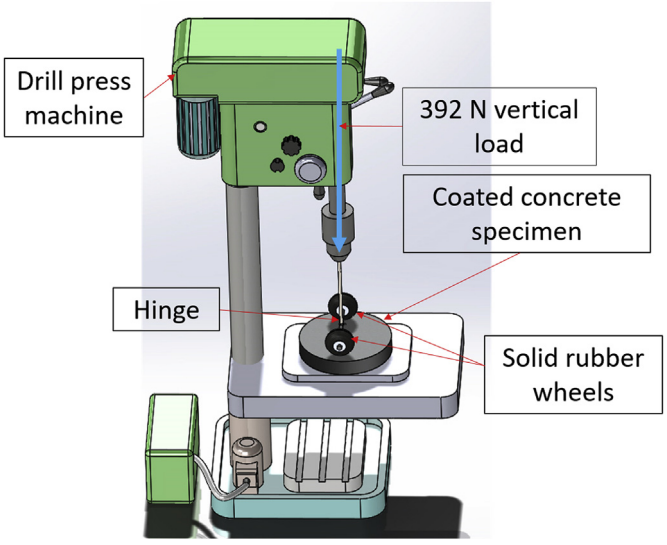

Fig. 3. Schematic of the coating durability test set-up.

and an electrically conductive filler [61]. Achieving high electrical conductivity in a composite material requires percolation of the conductive material through the insulating matrix. Therefore, the volume fraction of the conductive material (CMF in this study) should be equal to or greater than the value which enables the formation of a continuous path of fibers from edge to edge [67, 68, 71, 109]. The range of fiber content at which electrical conductivity abruptly increases is known as the percolation transition zone (or percolation threshold) [64].

Within the percolation transition range, by increasing the volume fraction of the conductive filler, the electrical conductivity of the composite rises by several orders of magnitude. Above percolation threshold, increasing the conductive filler dosage rate continues to improve the conductivity of the composite, but at a lower rate because the network of conductive filler is already saturated [61]. Excessive amount of conductive filler increases the mixture viscosity and makes it difficult to be uniformly applied on the substrate [61]. Therefore, the percolation transition zone of the CMF-PU composite was investigated through mixtures containing different volume fractions of CMF as shown in Table 1.

Using the mixture proportions given in the table, two types of coated specimens on wood and PCC substrates were prepared for measurement of electrical conductivity as shown in Fig. 1. Wood substrate was used because the electrical conductivity of dry wood is low enough to ensure there were no interferences with the conductivity measurements. Air-dried PCC substrate was used to simulate the real conditions in the intended application of these coating materials on PCC pavements. Since the results of the measurements on the two groups of specimens were comparable, the final electrical conductivity was taken as the average of the measurement results on both substrates (each specimen with three replicates).

Silver paste was applied to the two ends of specimens to be used as electrodes in measurement of resistance. Because the CMF, especially at low dosage rates, may not be exposed on the surface -reducing the electrical contact of the silver paste with the coating-the two ends of specimens were roughened -as shown in the figure-with scrub pad before applying the silver paste to improve the electrode-specimen contact. The two-probe method [110, 111], a reliable and accurate approach for resistance measurement, was utilized in this study, and the reason for reliability and accuracy of this method is thoroughly explained in the

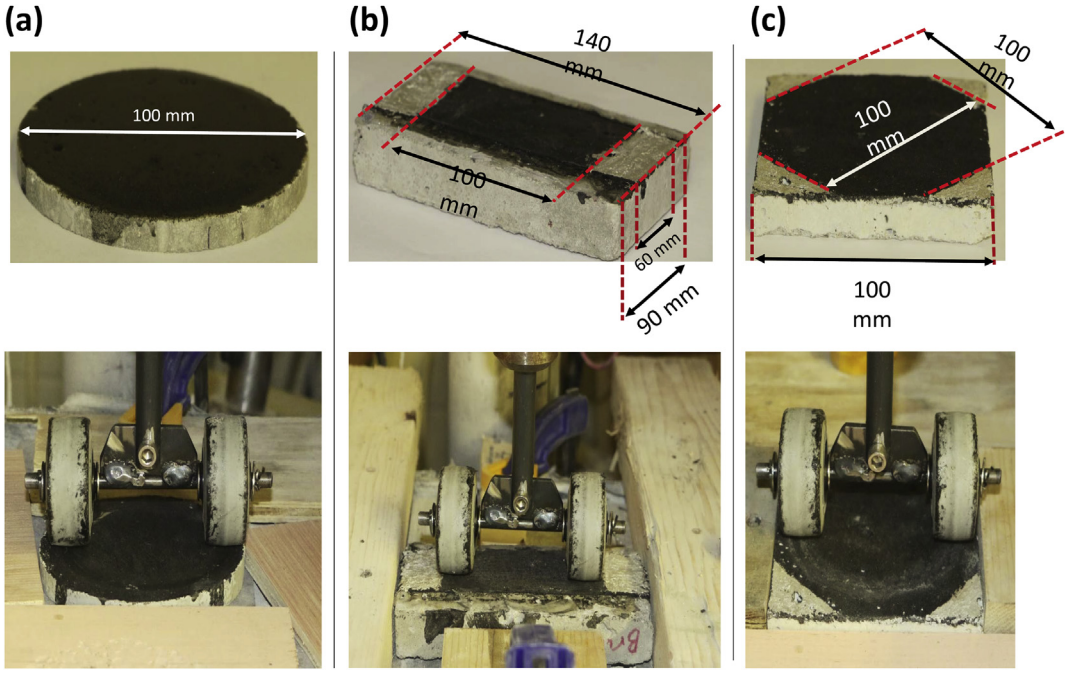

Fig. 4. Concrete specimens coated with PU-CMF composite and the test set-up for evaluating the (a) effect of loading cycle on mass loss, (b) effect of loading cycles-induced current flow path deterioration on electrical conductivity, (c) loading cycles-induced localized damage on electrical conductivity.

Table 2
Electrical conductivity of PU-CMF coatings containing different volume fractions of CMF.

CMF dosage rate (% Vol.)	Electrical Conductivity (S/cm)	Standard deviation	Relative standard error
0.25	3.28E-03	1.19E-04	2.09E+00
0.50	7.90E-02	1.38E-03	1.01E+00
0.75	1.97E-01	6.56E-02	1.92E+01
1.00	3.26E-01	5.77E-02	1.02E+01
1.50	3.26E-01	6.67E-03	1.18E+00
2.00	3.66E-01	7.61E-03	1.20E+00
2.50	4.22E-01	5.68E-02	7.77E+00
3.00	4.62E-01	7.35E-02	9.19E+00
3.50	5.59E-01	1.33E-01	1.37E+01
4.00	5.85E-01	1.02E-01	1.01E+01
5.00	3.18E+00	3.08E+00	5.59E+01
6.00	8.49E+00	1.88E+00	1.28E+01
7.50	1.59E+01	1.00E+00	3.64E+00
10.00	3.48E+01	7.69E+00	1.28E+01
12.50	3.71E+01	7.73E+00	1.20E+01
15.00	3.98E+01	2.34E-01	3.39E-01
17.50	4.19E+01	1.40E+01	1.94E+01
20.00	4.58E+01	7.19E+00	9.07E+00

authors' previous studies [1, 112]. A FLIR DM62 digital multimeter was used for measuring the resistance values. It is worth noting that the resistivity measurements were conducted using direct current (DC) for about virtually 1 s to avoid polarization [113]. All the measurements were performed at 20 °C and 30% relative humidity, in an environmental chamber, using the silver paste electrodes (Fig. 1). The environmental chamber, equipped with fans and a dehumidifier unit, ensured a uniform temperature and a minimum and constant amount of humidity in the air. Volume resistivity of pure water at 25 °C is about 18×10^6 Ω cm [114] and is reversely related to temperature. If the resistivity of water on the interface with coating surface is lower than that of the composite, a considerable electron flow occurs through water leading to error in resistivity measurement. The same condition prevails when the coating is implemented in the field, but other factors such as presence of different ions at variable concentrations, PH, etc. affect the electrical resistivity of water.

The thickness of coatings were measured with a thickness gauge (PosiTector® dry film thickness gauge with precision of 13–1000 μm); for each specimen, the thickness was measured on several spots and averaged to obtain the coating layer thickness. The width and length of each specimen between the electrodes were also measured with 0.01 mm precision. The dimensions of the coatings were used to calculate the volume resistivity in Ω-cm, and then, the volume conductivity (which is the reciprocal of resistivity) in S/cm was calculated according to Eq. (1):

$$\rho = R \frac{A}{l} \tag{1}$$

Where, ρ represents the electrical (volume) resistivity in ohm-centimeters (Ω-cm), R is the electrical resistance in Ohms (Ω), A is the cross sectional area normal to the current direction, and l is the distance between the two points with electrical potential difference of V. The electrical conductivity was plotted against the CMF dosage rate to determine the percolation transition zone.

To relate the electrical percolation results to resistive heating capability of the coatings, a heating test was performed on the wood-substrate specimens. An AC voltage of 5 V at a frequency of 64 Hz was applied to each specimen for the duration of 1 min. Meanwhile, the surface temperature of the specimen was measured and recorded using a FLIR T650sc Infrared camera, with a resolution of 640 × 480 pixels. The acquired radiometric data were then analyzed using the ResearchIR Max® software package, and the heat generation on the surface of each specimen for 1 min was quantified.

To evaluate the performance of the composite coating on concrete substrate in terms of resistive heating and durability, concrete specimens were coated with the PU-CMF composite at different CMF dosage rates which were selected based on the results of percolation threshold determination tests. The CMF dosage rates were selected such that the whole range of percolation transition zone and its vicinity were covered. The PU-CMF composite coatings used at this stage included 3, 4, 5, 6, 7.5, 10, 12.5, 15, 17.5, and 20% CMF by total volume of the composite. Each specimen was made in three replicates.

To evaluate the heating capability of the composites, rectangular concrete specimens with copper tape electrodes glued to the surface were prepared and coated as shown in Fig. 2. Heat generation efficiency of the composite-coated specimens were characterized through performing active IRT [107] at a temperature below the freezing temperature of water. To this end, all the specimens were preconditioned at -20 °C and 30% relative humidity for at least 3 h so they could achieve thermal equilibrium [108]. Because the PU used in this study is a hydrophobic material, the presence of moisture does not exert a significant effect on its

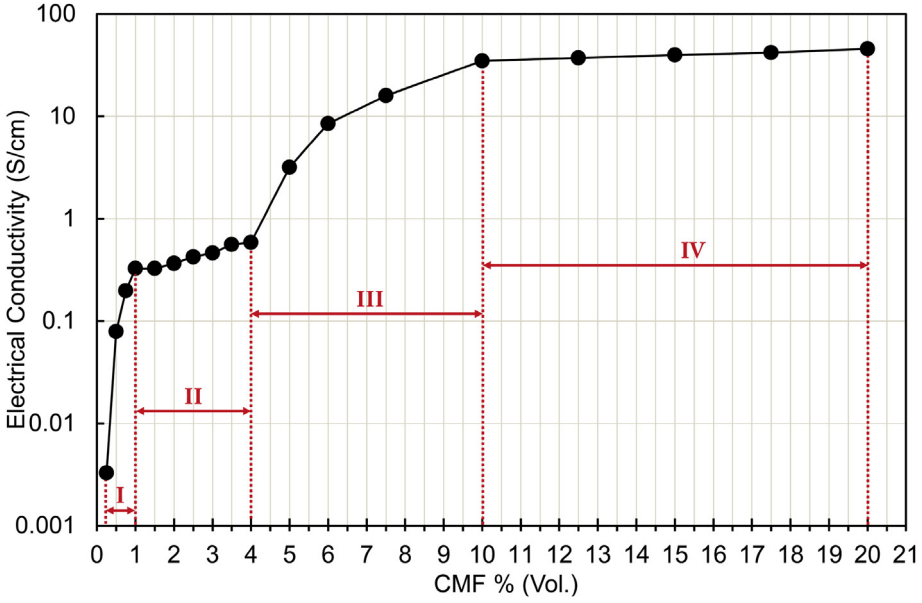

Fig. 5. Variation of volume conductivity with CMF dosage rate in the PU-CMF composite coatings.

electrical conductivity [115] and the presence of water on the surface either does not influence heating performance or tends to improve it by false reduction of volume resistivity as mentioned in the above. Therefore, the heating tests were performed at very low relative humidity inside the environmental chamber in order to avoid errors and make sure that the heat generation is accurately attributed to the coating material itself. An AC voltage of 20 V at a frequency of 64 Hz was applied to each specimen through the copper tape electrodes for a duration of 3 min. The surface temperature of each specimen was measured and recorded as explained above.

The durability of PU-CMF composite on PCC pavement surfaces was studied using the wheel path simulation test setup (Fig. 3) developed by Hawkins et al. [116] for studying the durability of pavement markings; this method is based on the abrasion resistance test (ASTM C944/C944M-12 standard) with some modifications that included using higher loads, applying the cyclic load by a different abrading tip (solid rubber wheels instead of rotating cutter), and using different specimen types.

Fig. 3 illustrates the coating durability test procedures by applying cyclic rotating wheel path at 250 rpm speed with 196 N force (1.66 MPa stress) vertical load under each wheel on three types of coated specimens. The mass loss of the coating materials, as a percentage of the mass of coating, was measured after 500, 1000, 5000, and 10000 cycles. Two types of specimens were used for investigation of the effect of cyclic loading on the electrical conductivity (electrical resistance) of coatings. Because of the changes made to the thickness and coverage area of coatings as the result of cyclic loading, the total electrical resistance of the coatings (instead of volume conductivity) before the test and after 10,000 loading cycles were used as the indicator of electrical durability. This approach helps eliminate the complications caused by cross sectional variations and evaluates the actual performance of the coating under load. Fig. 4(a) shows the specimens that were used for measuring the amount of the coating's mass loss after loading cycles. The specimens shown in Fig. 4(b), were used to simulate the situation where the entire width of the electric current flow path lies under the loading wheels. Fig. 4(c) shows the specimens that represent the case where the loading wheels travel on a fraction of the flow path between the electrodes; this approach was taken to investigate the effect of localized damage on the electrical conductivity of the whole coated surface. The change of electrical resistance after the loading was calculated by averaging the results obtained from the two types of specimens for each coating. The electrical resistance of the specimens shown in Fig. 4(c) were determined by making resistance measurements between each two diagonally opposite silver paste electrodes, repeating each measurement for three times on the same specimen, and taking the average of all readings as the electrical resistance of the specimen.

The effect of PU-CMF coating on skid resistance of concrete surfaces was investigated through measuring surface frictional properties of uncoated (control) and coated concrete specimens by British pendulum tester (BPT). British pendulum number (BPN), represents the amount of

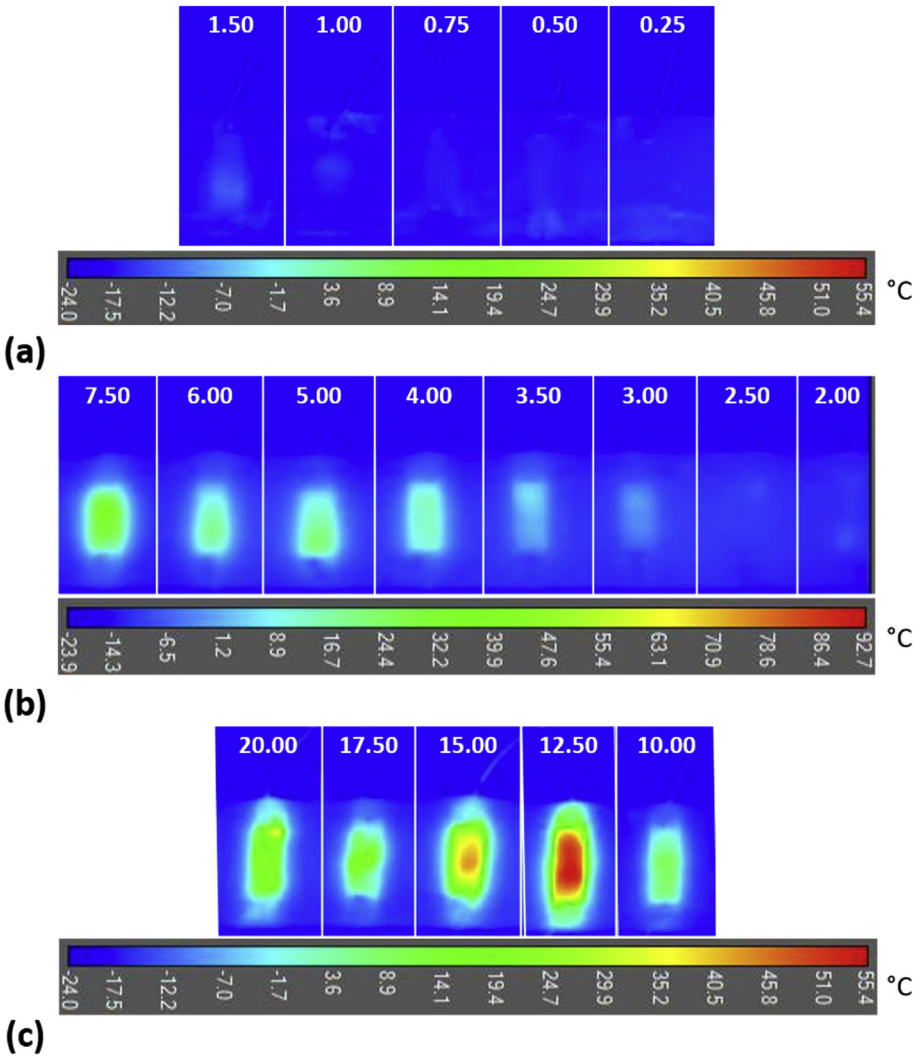

Fig. 6. Thermographic images of coatings with (a) 0.25–1.5%, (b) 2–7.5%, and (c) 10–20% CMF dosage rates on wood substrate after 1-minute current application.

kinetic energy loss after one pass of BPT rubber slider on a test surface [52]. Higher BPN indicates higher skid resistance of the surface. Similar to the authors' previous study [24], the ASTM E303-93 standard [117] practice for measuring surface frictional properties by BPT was followed except that, unlike the standard procedure where skid resistance is measured only on wet surfaces, the tests were performed on both wet and dry surfaces for the sake of comparison. Coated specimens were similar to that shown in Fig. 2 coated with PU-CMF composites at CMF dosage rates similar to the aforementioned concrete-specimen heating test. Control specimens were of the same geometry, material, and surface texture of the coated concrete specimens. The test was repeated three times on each specimen and the average BPN was recorded to represent skid resistance. The skid resistance tests were performed at ambient conditions of 23 °C and 65% relative humidity.

2.2. Cost analysis

Due to lack of full-scale construction of heated pavements made of conductive coatings, there was no attempt to develop a standardized cost estimation for construction of this snow removal technology. In this study, the construction cost and material cost of the heated pavements made of conductive coatings were estimated using conceptual cost estimation method that is a stage of design with limited component information [118, 119]. Although, project-level cost estimation would provide further insights and information about the construction costs associated with this technology, due to lack of availability of the cost data regarding the full-scale implantation, project-level cost analysis is not a doable option at this stage. To enhance the construction cost estimation accuracy and precisions, the construction costs analysis used in a previous paper on economic performance of electrical concoctive concrete

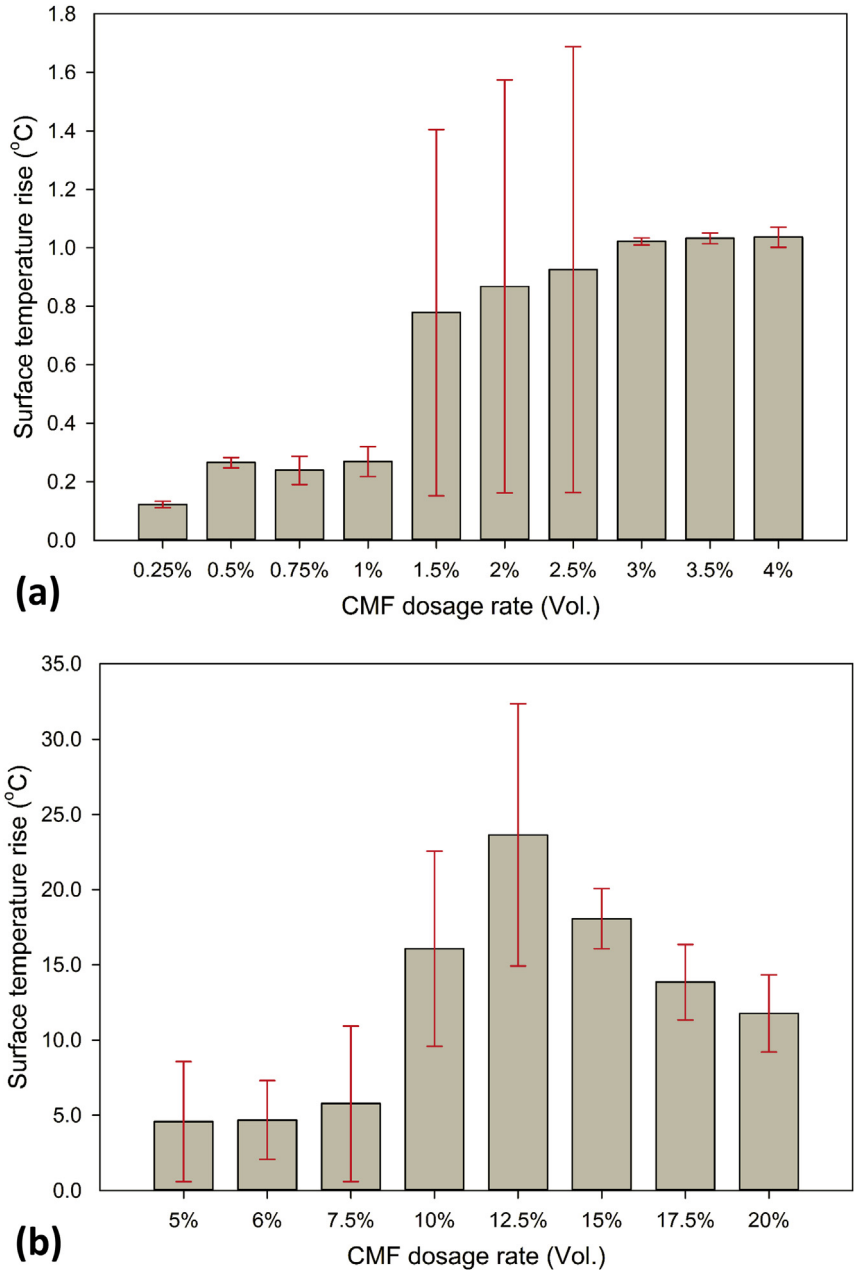

Fig. 7. Average surface temperature rise of coatings on wood substrate at CMF dosage rates (a) below and (b) above the lower limit of second percolation transition zone after 1 min of current application.

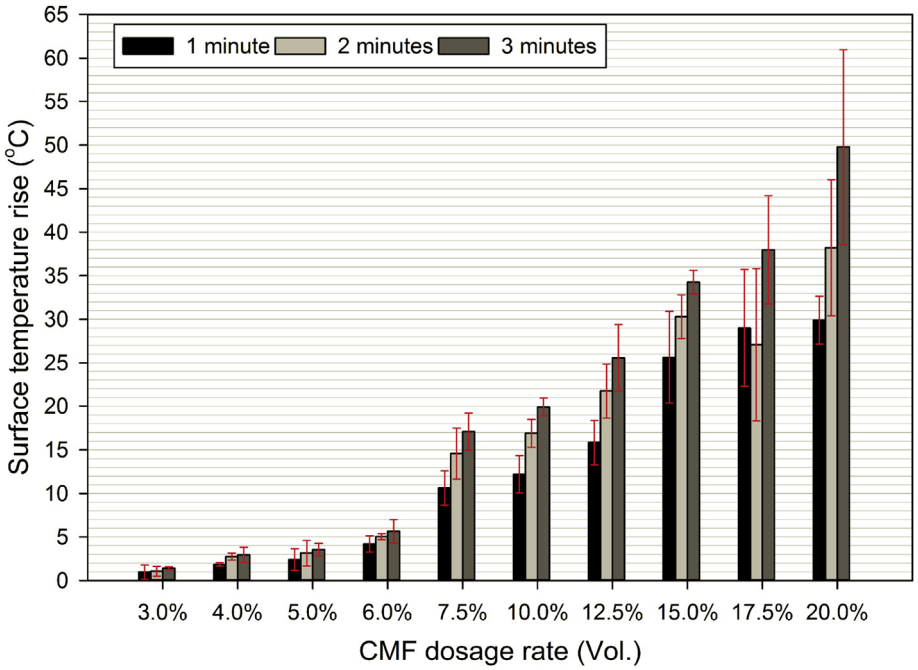

Fig. 8. Average temperature rise on the surfaces of coated concrete specimens at different durations of electric current application.

systems (ECON HPS) was used as the base line of the costs analysis. To this end, the costs associated with electrodes, wiring, and power supply were obtained from a previous study. In addition, the construction activities were divided into two different types of activities: (I) activities which are in common with full scale construction of the ECON HPS, and (II) construction activities that are different from ECON HPS implementation. Lastly, as mentioned in the introduction section, To provide some insight, the costs associated with the materials and the construction of a heated pavement system made of conductive asphalt concrete were compared with those of conventional asphalt concrete.

3. Results and discussion

3.1. Experimental results

Table 2 shows the volume conductivity of PU-CMF coatings with different volume fractions of CMF and the results are visualized in Fig. 5. As seen in Fig. 5, the selected range of CMF content resulted in fully capturing the percolative behavior [120], such that the dual critical percolation threshold was found [121]. As seen in the figure, four different zones can be distinguished in the "*conductivity-CMF dosage*" plot that include two abrupt increase zones and two plateauing regions. The first sizeable increase of volume conductivity occurred in Zone I, between 0.25% and 1% CMF volume fractions, which shows the transition of the composite from insulator to semiconductor. In zone II, the curve plateaued, until the second abrupt jump occurred in zone III between 4% and 10% CMF volume fractions; this corresponds to the percolation transition zone over which the composite transfers from a semiconductor into a conductor [121, 122]. As per the definition of percolation transition zone, by increasing of CMF dosage rate above the "*semiconductor-to-conductor*" percolation transition range (4–10% Vol.), the volume conductivity is marginally increased as depicted by zone IV in the figure. In the work conducted by Wu et al. [121], with a graphite/high-density polyethylene composites, the two percolation transition zones were found at filler dosage rates of 12.29% (Vol.) and 21.79% (Vol.) respectively. This finding reveals a more effective percolation behavior of CMF compared to graphite powder.

As seen in Table 2, the relative standard error was higher relative to the neighboring points -i.e. 1% and 4 % CMF dosages-that correspond to the turning points between the zones in Fig. 5. This observation is in agreement with the findings of previous work [120, 123] postulating that the electrical conductivity of different specimens with the same conductive filler is higher before the formation of continuous conductive network, especially at the proximity of percolation threshold.

Figs. 6 and 7 show the heating capability of PU-CMF coatings on wood substrate after 1 min of current application. Up to 12.5% CMF

Table 3
Thermography results for PU-CMF-coated concrete specimens.

CMF dosage rate (%Vol.)	Duration (minutes)					
	1		2		3	
	Temperature (°C)	Standard Deviation	Temperature (°C)	Standard Deviation	Temperature (°C)	Standard Deviation
3.0	1.0	0.8	1.1	0.6	1.4	0.2
4.0	1.9	0.2	2.8	0.4	3.0	0.9
5.0	2.4	1.3	3.2	1.5	3.5	0.7
6.0	4.2	0.9	5.0	0.3	5.7	1.4
7.5	10.6	2.0	14.6	2.9	17.1	2.1
10.0	12.2	2.1	16.9	1.6	19.9	1.0
12.5	15.8	2.5	21.8	3.1	25.6	3.8
15.0	25.6	5.3	30.3	2.5	34.3	1.3
17.5	29.0	6.7	27.1	8.8	38.0	6.2
20.0	29.9	2.7	38.2	7.8	49.8	11.2

dosage rate, the average surface temperature, at the end of electrical heating test, increased with CMF volume fraction. Above 12.5% CMF dosage rate, the trend was reversed resulting in a reduction in heat generation capability. The abrupt jump in the surface temperature rise at 1.5% CMF dosage corresponds to the first point after the "*insulator-to-semiconductor*" percolation transition zone. The measured values exhibited a higher variation in the vicinity of each of the three turning points (1%, 4%, and 10% CMF) which correspond to the transitions between the different zones of Fig. 5. However, because of the complicated viscoelastic behavior of the composite at filler dosages at or near the percolation transition zones [121], this behavior cannot be merely attributed to the fluctuations of volume conductivity. Rather, the quality of the coating with respect to surface application uniformity also affects the ability of heat generation.

Fig. 8 and Table 3 present the average temperature rise on the surface of concrete specimens coated with PU-CMF composites of different CMF volume fractions; the heating behaviors are shown at three different durations of electric current application (1, 2, and 3 min). At all three time intervals, the average surface temperature assumed an increasing trend with increase of CMF dosage rate. An abrupt jump in heat generation occurred at 7.5% CMF, such that, after 3 min of electric current application, the average temperature on the surface of 7.5%-CMF specimen was about three times higher than the specimen coated with 6%-CMF composite.

Fig. 8 shows a continuous increase of "*average surface temperature rise*" with CMF dosage rate. Comparing Fig. 8 with Fig. 6 and Fig. 7, one may conclude that the results obtained from heating test on composite-coated concrete specimens contradict those obtained from small wood-substrate specimens. However, the thermographic images of concrete specimens at critical CMF dosage rates, i.e. 3%, 6%, 7.5%, 10%, 12.5%, 15%, and 17.5% that are shown in Fig. 9 cast a light on what appeared to be a discrepancy between the heat generation results obtained from the two experiments. As seen in Fig. 9, with CMF dosage rates up to 12.5%, the temperature distribution on the coated surfaces between the two electrodes were almost uniform without any extreme heat concentration spots. Whereas, at 15%, and 17.5% CMF contents, the electrical-energy-to-heat-energy conversion occurred at a small fraction of the coating, significantly increasing the temperature at some spots and leaving the majority of the surface unheated. This heat concentration can be attributed to high variation of electrical-resistivity between different zones of the coating layer due to poor CMF dispersion. At high CMF contents, the composite is more susceptible to filler agglomeration; however, this is hard to capture in small specimens like those used to obtain Figs. 6 and 7. Using the mixing and dispersion procedure of this study, the optimum CMF dosage rates with respect to resistive heating capability, is assumed to be greater than 7.5% and smaller than 15%. PU-CMF composites containing 10% and 12.5% (Vol.) conductive filler provided desirable performance with regards to both the magnitude of average temperature increase and the temperature distribution uniformity. In absence of CMF agglomeration and high-resistivity zones in the coating, the temperature uniformity was improved by time as the heat was dispersed within the coating layer. Whereas, in the specimens that contained CMF dosage rates greater than 15% where coating uniformity was not desirable the heat distribution became more non-uniform by time. This can be attributed to increased heat concentration on the high-resistivity zones to the level that could not be nullified by heat dispersion resulting in more severe non-uniformity of heat distribution. It is hard to say if the heat concentration spots are the high-resistivity or low-resistivity zones,

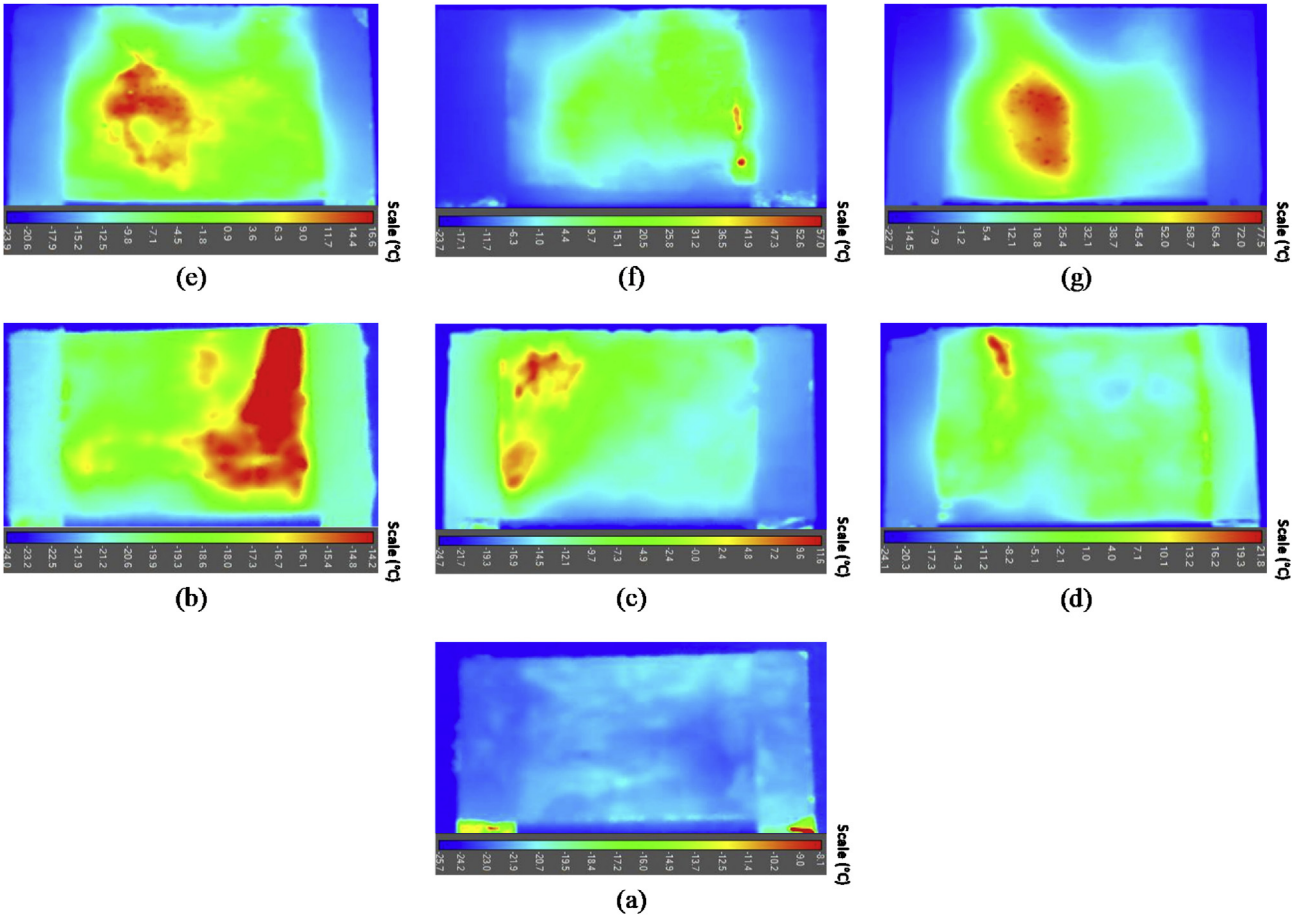

Fig. 9. Infrared thermal images after 3 min of electric current application for concrete PU-CMF-coated specimens at CMF dosage rates of (a) 3%, (b) 6%, (c) 7.5%, (d) 10%, (e) 12.5%, (f) 15%, and (g) 17.5%.

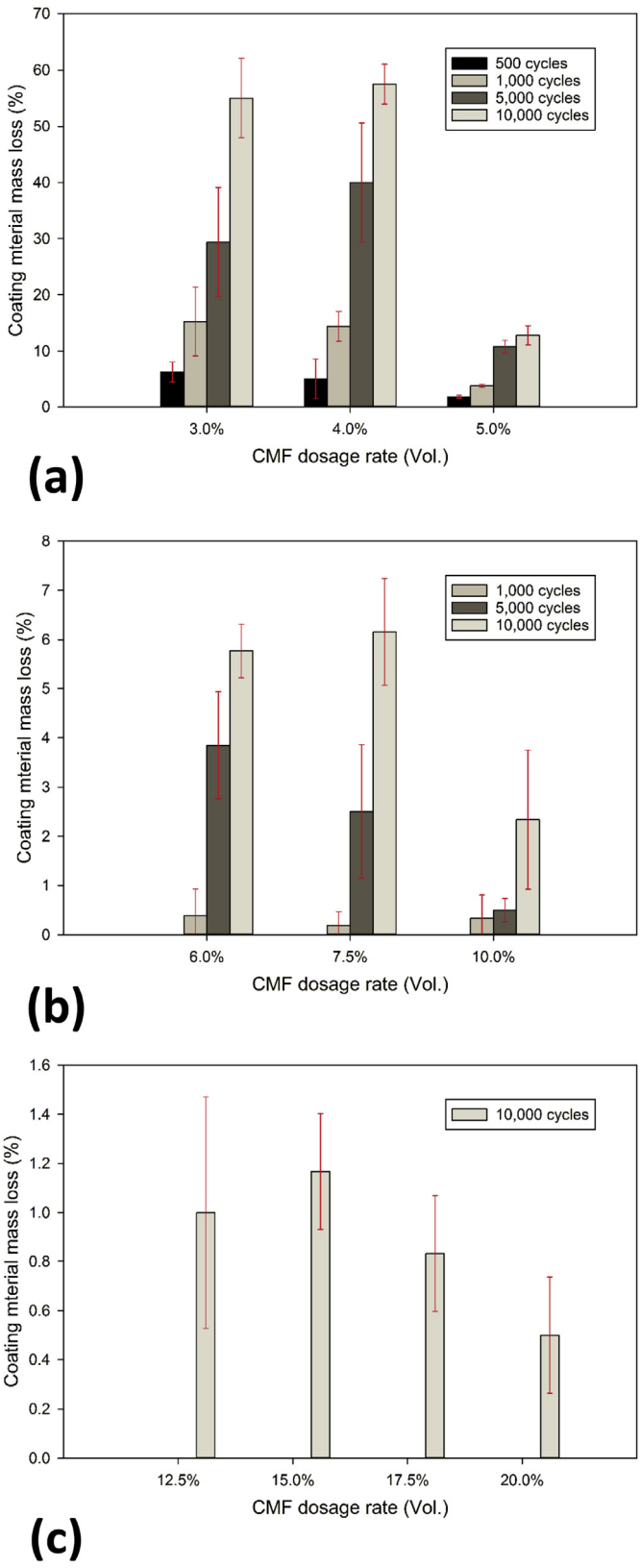

Fig. 10. Mass loss of coatings with different CMF dosage rates. Coatings showing measurable mass loss at (a) all; (b) greater than 500; and (c) greater than 5,000 loading cycles.

because the amount of heat generation depends on both the current flow and resistivity which are also reversely related to each other. An extreme case was observed in the heating tests of one of the 17.5%-CMF specimens. When this specimen was tested for its heat generation capability, at the beginning of the test the whole surface was heated, but excessive heat concentration after about 1 min resulted in loss of bond between the electrode and the coating at a fraction of the electrode's length resulting in temperature decrease on its adjacent coating area. This is the reason for the drop of average temperature rise after 2 min seen in Fig. 8. This temperature drop was compensated after 3 min by increase of heat concentration in the rest of the specimen that was still in the circuit and the average surface temperature rise increased as seen in the figure. The authors did not discard this specimen to highlight the negative effect of coating non-uniformity on heating performance.

The amount of mass loss undergone by the PU-CMF coatings when subjected to cyclic loading is shown in Fig. 10. Increasing CMF volume fraction from 3% to 4% resulted in smaller mass loss at 500 and 1,000 loading cycles, while, this trend was reversed at 5,000 and 10,000 cycles with the coatings containing 4% CMF exhibiting greater mass loss. As seen in Fig. 10(a), there was a significant drop in the amount of coatings' mass loss at the CMF volume fraction of 5% which corresponds to the beginning of percolation transition zone (second transition zone in Fig. 5). At CMF-dosage rates higher than 5% (Fig. 10(b) & (c)), the loss of coatings' mass under cyclic load at all test durations was decreased with increasing the CMF volume fraction. As seen in Fig. 10(b), in the range of 6%–10% CMF content, no measurable amount of coating materials were lost at 500 loading cycles while the mass loss at 1,000 cycles was also negligible. Above 10% CMF content, shown in Fig. 10(c), the coatings lost none of their mass up to 5,000 cycles of loading and a very small mass loss was observed at 10,000 cycles. This observation indicates that the CMF network contributes to the strengthening of Polyurethane matrix and improves its durability.

The results of electrical resistance measurement on coatings before and after 10,000 cycles of loading, shown in Fig. 11(a) & (b), confirmed the positive effect of CMF on durability of coatings. It was observed that up to 6% CMF dosage rate, the electrical conductivity of the coatings was severely degraded resulting in a marked increase in electrical resistance. Increasing CMF dosage rate above 6%, as seen in Fig. 11(a), improved the coatings' durability and diminished the increase of resistance after loading by orders of magnitude. At 7.5% and 10% CMF contents, the electrical resistance after 10,000 load cycles was, respectively, 3 times and 9 times greater than its initial value before load application. When CMF dosage rate was increased to values higher than 10% - virtually the percolation threshold-the electrical resistance after 10,000 cycles of wheel path was even lower than its initial value resulting in negative values of resistance change in Fig. 11(b)). Note that the coatings containing 12.5, 15, 17.5, and 20% CMF showed a negligible amount of mass loss after 10000 load cycles (shown in Fig. 10(c)); therefore, the coating layer remained completely intact after the load application and the cross sectional area of the coating available for passing the current was not significantly reduced.

For a material with a certain volume resistivity, the electrical resistance is directly proportional to the distance between electrodes and reciprocal of the cross sectional area in the direction of current. As seen in Fig. 12, the specimen coated with 10%-CMF coating was torn apart by cyclic wheel path and lost its electrical continuity, while, the 15%-CMF coating stayed completely intact. It is also seen in the figure, that in the durable coatings (e.g. 15%-CMF) the coating materials were to some extent compacted in the wheel path. The compaction of coating tends to bring the CMF fibers closer to each other and boost the fiber-to-fiber contact. Also, smaller spacing between fibers tends to increase the chance of electron hopping (tunneling effect) between non-contacting fibers. The one-by-one contact between conductive fibers and the electron hopping between fibers that are not in direct contact with each other are among primary mechanisms of conduction in electrically conductive fiber-matrix composites [124, 125]. With respect to the observation that the reduction of cross sectional area above 10% CMF content was negligible (Fig. 10(c)), its negative effect on electrical conductivity was possibly dominated by the positive effect of compaction resulting in

reduction of electrical resistance in Fig. 11(b).

The results of investigating volume resistivity variation with CMF dosage rate (0.25%–20% Vol.) captured the dual percolation transition zone at 0.25%–1% for *insulator-to-semiconductor* and 4%–10% for *semiconductor-to-conductor* transitions respectively. Heating capability tests on PU-CMF composites using two types of specimens indicated that the heating efficiency of the coatings experiences significant improvement at two thresholds of 1.5% and 10% CMF, while at CMF dosage rates higher than 12.5% the small specimens showed reduction of heating ability and larger specimens showed lack of heat distribution uniformity. The durability of coating was continuously improved by increasing the CMF volume fraction, with two abrupt jumps at 5% and 12.5%. Regarding these results, CMF volume fraction greater than 10% and smaller than 15% can be identified as the desirable range for dosage rate of CMF conductive filler in the PU-CMF composite in terms of electrical conductivity, electrical heating capability, and durability.

Since the mixing, application, and performance testing temperatures were kept constant in this study, it is worth mentioning that the electrical heating performance of PU-CMF coating is affected by temperature-related factors at production, application, and service levels. Because the rheological properties of the PU component is temperature-dependent, the temperature at which the mixture is prepared exerts a significant influence on the quality of dispersion of CMF in the PU continuum, and consequently, on the conductivity and uniformity of the composite. This also applies to the temperature of the mixture during surface application. Furthermore, the electrical conductivity of the material is changed by temperature, depending on its temperature coefficient [90, 115] that can impart thermistor or posistor properties to the material. As long as the in-service temperature is concerned, the durability of the coating is also likely to be affected. The influence of

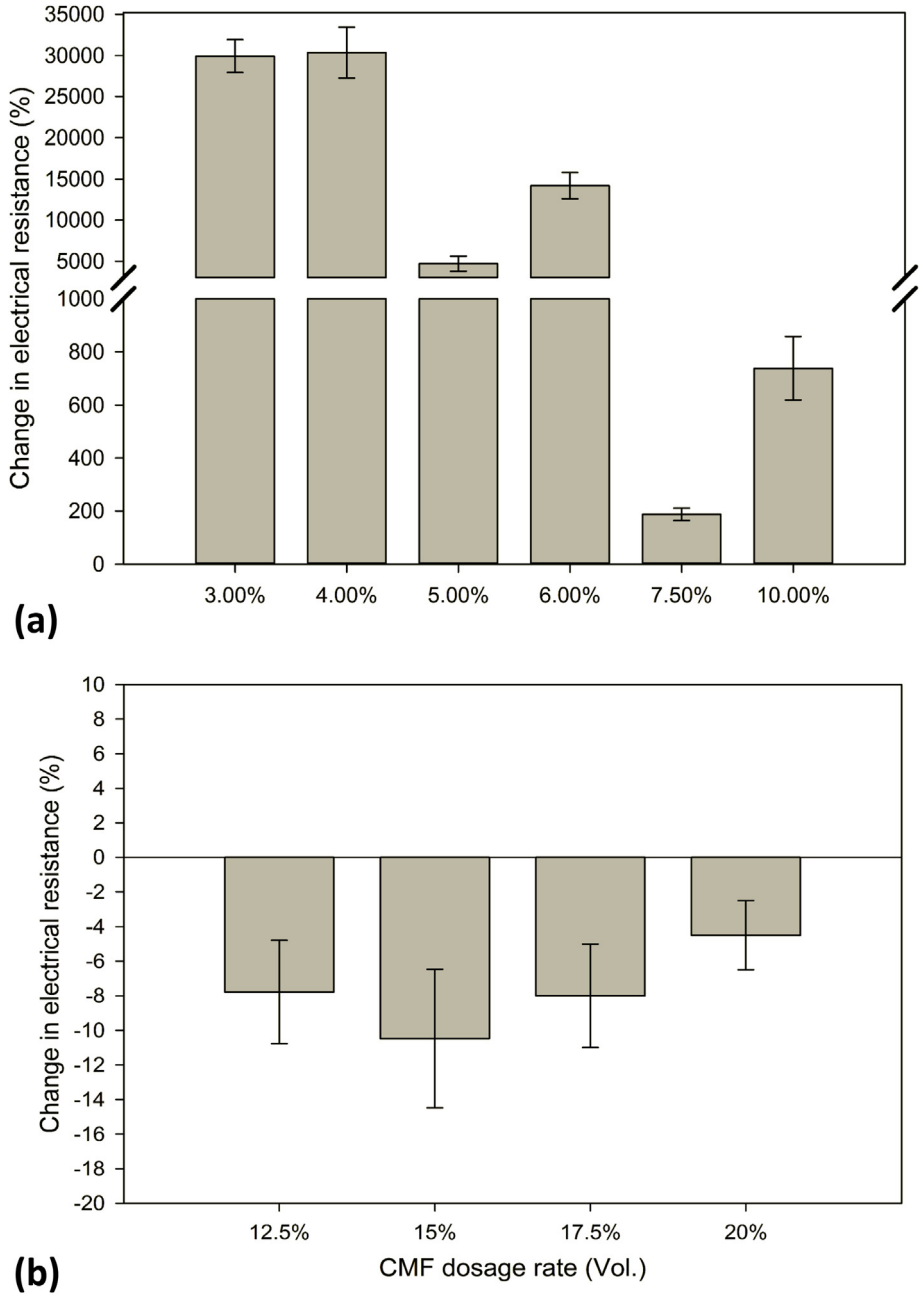

Fig. 11. The changes in electrical resistance of coatings after 10,000 loading cycles for (a) coatings that experienced resistance increase, and (b) coatings that experienced resistance decrease.

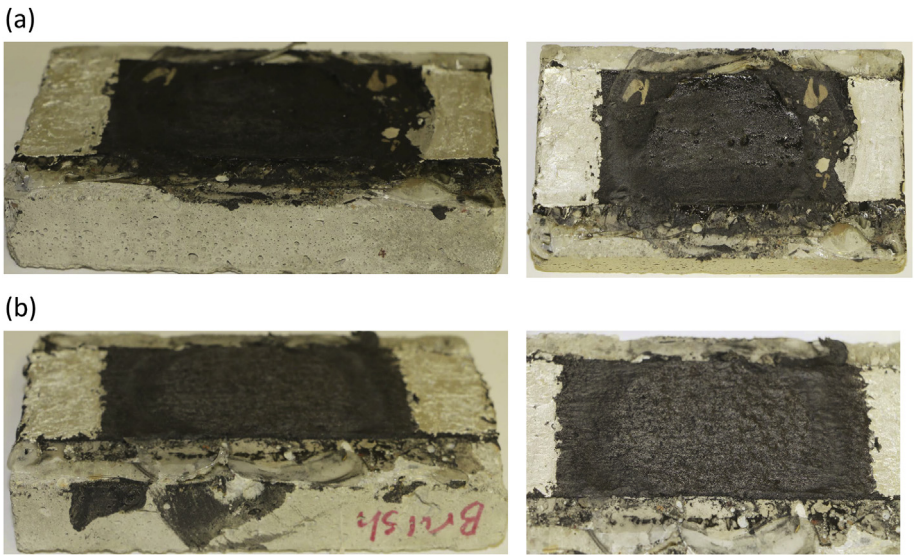

Fig. 12. PU-CMF coatings with (a) 10%, and (b) 15% CMF dosage rates after 10,000 loading cycles.

temperature at different stages of production, application, and service and its relation to the performance of different PU-CMF composites need to be investigated in future studies.

Fig. 13 shows the BPN for the control and coated specimens at different CMF dosage rates in dry and wet surface conditions. As seen in the figure, coating the specimen with a PU-CMF composite that contained 3% CMF resulted in dramatic reduction of skid resistance, but the BPN exhibited an increasing trend by increasing the CMF dosage rate. As long as the CMF dosage rate was smaller than 7.5% the coatings reduced the skid resistance of concrete specimen, while both dry- and wet-surface skid resistance were greater than the control specimen when CMF content was equal to or greater than 10%. It can be concluded that when CMF dosage rate of the PU-CMF composite coating is lower than percolation threshold the skid resistance is reduced by coating, and when the CMF dosage rate is higher than percolation threshold, the skid resistance of a coated concrete surface is higher than its equivalent plain (uncoated) concrete surface. This observation can be explained by the dominance of PU component -that has very low friction-below percolation threshold and the dominance of the high-friction CMF component after percolation. All specimens showed higher skid resistance, i.e. greater BPN, at dry surface conditions while the difference between dry and wet BPN was affected by the CMF dosage rate. At CMF contents equal to or greater than 10%, dry- and wet-surface BPN values showed a small difference that was even smaller than those observed in control specimens.

3.2. Cost analysis

Material costs of heated pavement system made of conductive coatings were estimated based on the following assumptions:

a) The material costs associated with the conductive coating materials were estimated based on the cubic meter of the raw material used for the mixture
b) Cost of 10 cm conventional Portland cement concrete substrate layer was also included in the material cost estimation
c) Cost of Polyurethane (PU) ≈ 4,700 (USD/m^3)
d) Cost of carbon micro filler (CMF) ≈ 24,000 (USD/m^3)
e) The coating thickness is 3mm (1/8 inch)

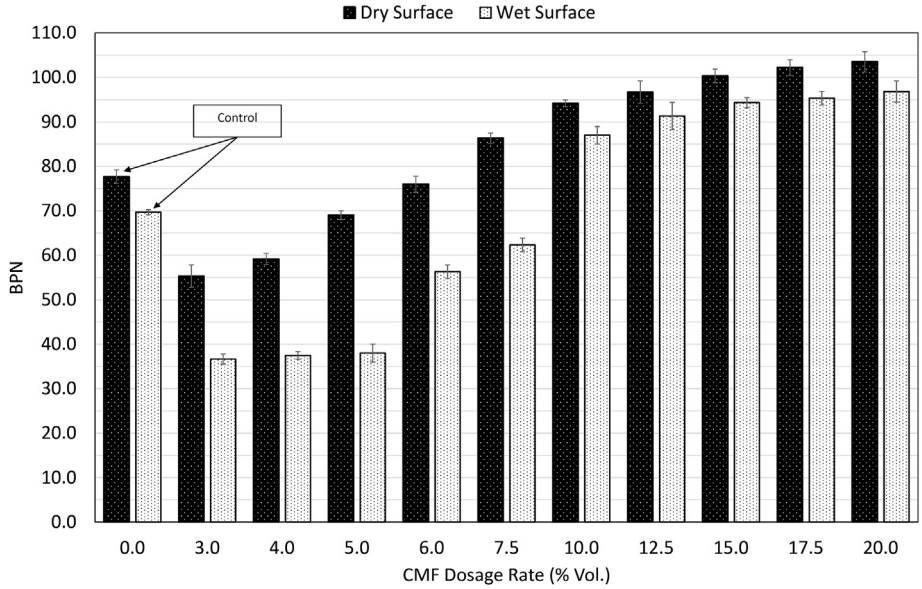

Fig. 13. British pendulum test results for the control and coated concrete specimens.

Table 4
The conceptual material costs estimation for the conductive coating (the table is created based on a previous study on ECON HPS economic performance [103]).

Materials	Material Costs for PCC, 10 cm base layer (USD/m^3)	Material Costs for ECON HPS (USD/m^3)	Material cost of heated pavement system made of conductive coatings (USD/m^3)
Polyurethane (PU)*	-	-	15
Carbon micro filler (CMF)*	-	-	75
Carbon fiber	-	110	
Coarse aggregate	36	36	36
Fine aggregate	10	10	10
Cement	84	84	84
HRWR (high range water reducing admixture)	-	0.005	-
AEA (air entraining admixture)	-	0.25	-
Conductivity enhancing agent	-	0.25	-
Dispersive agent	-	29	-
Total	130	270	220

* Cost of Polyurethane and CMF were obtained directly from the manufacturer.

Also the estimated material cost of the conductive coating compared with conventional Portland cement concrete and ECON HPS.

According to Table 4, material cost of conductive coating is almost 70% higher than the conventional concrete. The major difference between cost of the conductive coating materials and conventional concrete is mostly related to the use of CMF in conductive coating. In addition, material cost of ECON HPS is almost 20% higher than the materials for heated pavement made by the conductive coating.

Material cost estimation enables the construction cost estimation of the heated pavement systems made by the conductive coating. To this end, a work break-down structure (WBS) was constructed to divide construction activities to four different work packages (Fig. 14).

As shown in Fig. 14, among all the major construction activities, five of the work packages were in common with ECON HPS. To this end, the costs associated with these work packages were considered to be same as cost for heated pavement made of conductive coating. Also cost for coating pavement surface with conductive materials were estimated based on the material cost obtained from Table 4. In addition, labor cost for coating the pavement surface was assumed to be same with the pavement marking, which was obtained from RSMeans construction cost index [126]. Table 5 presents the construction costs estimation for heated pavement made of conductive coating for a 17.5 m^2 slab (5 m $\times$ 3.5 m).

According to Table 5, the installation cost of a heated pavement system made of conductive coating is almost the same with ECON HPS, which is almost 50% higher than construction cost of conventional Portland cement concrete [103]. The construction cost of implementing conducting coating is relatively high. But for some specific applications, conductive coating heated pavements might be an economic option (e.g., on the airports with high number of aircraft operations which experience harsh winters [102] or on a bridge deck with high accident rate during winter seasons [104]).

Fig. 15 compares the construction cost of heated pavement made of conductive coating with reported construction cost of three other heated pavement systems. As exhibited in Fig. 15, the construction cost of heated pavement made of conductive coating is almost the same as installation cost of ECON HPS and very close to the median value of reported cost of construction cost of hydronic heated pavement systems (HHPS). Also, the construction cost for electrically conductive asphalt concrete (ECAC) was estimated to be almost 300 USD/m^2 [127] which is almost 30% lower than heated pavement made of conductive coating. This cost difference mainly relates to the lower cost of asphalt concrete used in ECAC (rather than the higher cost associated with regular Portland cement concrete used in heated pavement made of conductive coating). In addition, cost of heated pavement made of conductive coating is more than two times

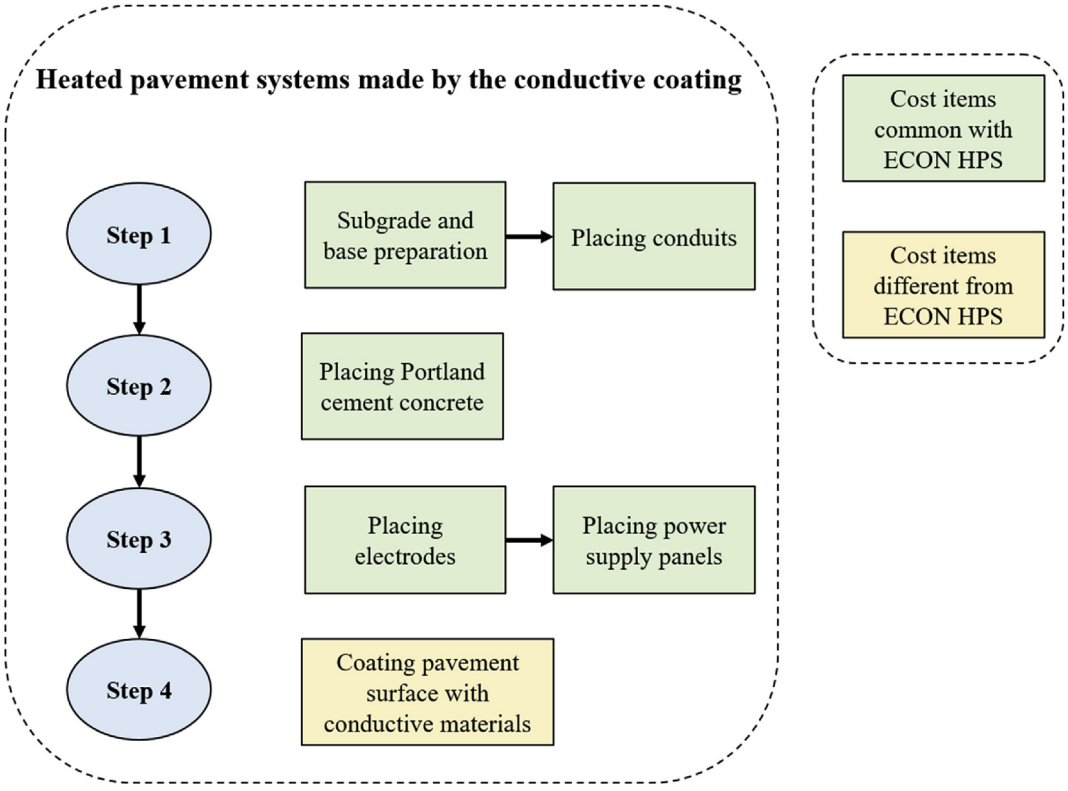

Fig. 14. WBS of heated pavement system made of conductive coatings vs. WBS of ECON HPS (Created based on the previous study on economic performance of the ECON HPS [103]).

Table 5
Construction cost of ECON HPS vs. construction cost of heated pavement made of conductive coating.

		Item	Unit	Quantity	Unit Price (USD)	Total (USD)
Common factors		Subgrade preparation	m^2	17.5	38	665
		Crushed aggregate base course, 8in.	m^2	17.5	25	437
		Placing dowel baskets	EA	8	65	520
		Electrodes (electrode size 2.5 cm x 2.5 cm x 3.5m)	EA	6	65	390
		Installing power supply box	EA	1	750	750
Common factors	ECON HPS	10 cm PCC Pavement	m^2	17.5	100	1,750
		9 cm ECON	m^2	17.5	165	2,887
	Conductive coating	19 cm PCC Pavement	m^2	17.5	150	2,625
		3 mm conductive coating application	m^2	17.5	110	1,925
Total construction cost for ECON HPS (USD)						7,400
Total cost for heated pavement made of conductive coating (USD)						7,312
Total cost for heated pavement made of conductive coating (USD/m^2)						418

less than construction cost of geothermal heating pavement systems. The major cost difference between the conductive coating heated pavement and geothermal systems relates to the heating source installation and material costs.

4. Conclusions

Electrically conductive composites of Polyurethane (PU) and carbon microfiber (CMF) were prepared using different volume fractions of the conductive filler (CMF) and tested for their electrical conductivity, heating capability, and durability on Portland cement concrete (PCC) substrates under cyclic loaded wheel path. The electrical conductivity was evaluated in terms of percolation of microfibers within the PU matrix. Heating capability tests included investigation of the average surface temperature rise and temperature distribution over the surface area of the composite-coated specimens upon application of electric current on wood-substrate and PCC-substrate specimens. Durability of coatings on PCC-substrate was assessed in terms of coating layer's mass loss and electrical resistance change under certain cycles of loading through loaded wheel path. The main findings of the study can be summarized as:

- Applying the coating materials that contained different dosages of CMF on wood and concrete substrates, the dual percolative behavior of the CMF in PU matrix was captured in the studied range. The percolation transition zone in the 0.25%–1% range corresponds to transition of the composite's behavior from electrical insulator to semiconductor. The composite transitioned from a semiconductor to a conductor of electricity over the CMF dosage rate range of 4%–10% above which the volume conductivity did not exhibit significant improvement with the increase of CMF content.
- Resistive heating test on coated wood-substrate specimens showed that increasing CMF volume fraction from 1% to 1.5% resulted in an abrupt jump in resistive heat generation. The second significant improvement of heating capability occurred at 10% CMF dosage rate. Increasing CMF content of the composite above 12.5% led to reduction of heating performance in terms of the average surface temperature rise.
- In coated concrete-substrate specimens, that had larger area than the wood-substrate specimens, the average surface temperature rise continuously increased with CMF dosage rate between 3% and 20%. The abrupt jump in surface temperature rise occurred when CMF dosage was increased from 6% to 7.5%. Increasing CMF content of the composite above 12.5% led to reduction of heating performance with respect to the uniformity of temperature distribution.
- The durability of composites continuously improved with increasing CMF volume fraction up to 20%. However, the most desirable durability properties were achieved at CMF contents higher than 10%.
- At CMF dosage rates below the percolation threshold (10%), the coating reduced the skid resistance of the concrete substrate and at dosage rates equal to or greater than percolation threshold, coated

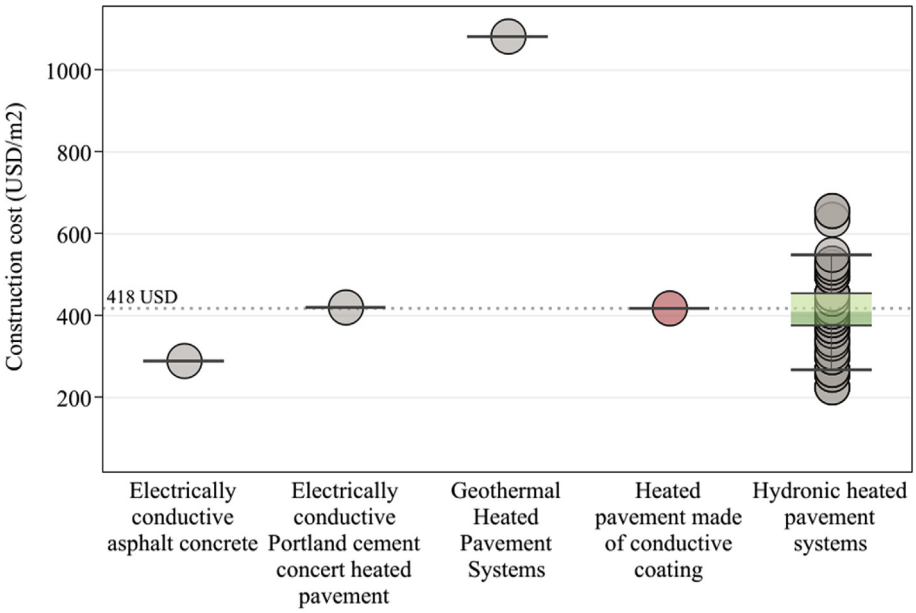

Fig. 15. Construction cost comparison among various heated pavement technologies (created based on the data obtained from literature [102, 103, 104, 127, 128]).

surfaces showed higher skid resistance than the uncoated concrete substrate at both dry and wet surface conditions. The skid resistance of composites continuously improved with increasing CMF volume fraction up to 20%.

- Considering all four characteristics of the coating -i.e. volume conductivity, heating capability, durability and skid resistance-within the studied range of CMF volume fraction, the composites containing 12.5% CMF content exhibited more favorable properties than other coating mixtures. It can be concluded that a CMF dosage rate greater than 10% and smaller than 15% (by total volume of the composite) is likely to be the desirable range of CMF volume fraction in the PU-CMF composite studied in this research.
- Construction cost of heated pavement made of conductive coating is almost fifty percent higher than regular Portland cement concrete, but comparable to the heated pavement technologies that use electrically conductive Portland cement and asphalt concretes or hydronic systems. Although the construction cost of heated pavements still is relatively high, it is expected that advances in heated pavements materials design and selection and implementation techniques can reduce the initial construction cost of heated pavement made of conductive coating.

Regarding the desirable properties of the PU-CMF composite studied in this research, it would be timely for future studies to investigate different types of binders such as various Polyurethane/Polyurea elastomers and Poly (methyl metacrylate) to produce more durable electrically conductive coatings for different substrates and applications. Doping PU-CMF composites with different nano- and micro-particles or fibers is a potential topic for future studies to impart additional functions, other than electrical conductivity, to this type of composites. Other applications of these composites such as sensing and electromagnetic interference shielding can be investigated in the future studies. Investigating different dispersion improvement methods to enhance the uniformity and conductivity of the PU-CMF composites is a potential topic for future works that will make a significant contribution to the existing body of knowledge on this subject.

Data availability

The raw/processed data required to reproduce these findings cannot be shared at this time as the data also forms part of an ongoing study.

Declarations

Author contribution statement

Alireza Sassani, Ali Arabzadeh: Conceived and designed the experiments; Performed the experiments; Analyzed and interpreted the data; Contributed reagents, materials, analysis tools or data; Wrote the paper.

Halil Ceylan, Sunghwan Kim: Contributed reagents, materials, analysis tools or data.

Kasthurirangan Gopalakrishnan, Peter Taylor, Ali Nahvi: Analyzed and interpreted the data; Wrote the paper.

Funding statement

This work was supported by the Federal Aviation Administration (FAA) Air Transportation Center of Excellence Cooperative Agreement 12-C-GA-ISU for the Partnership to Enhance General Aviation Safety, Accessibility and Sustainability (PEGASAS).

Competing interest statement

The authors declare no conflict of interest.

Additional information

No additional information is available for this paper.

Acknowledgements

This paper was prepared from a study conducted at Iowa State University under Federal Aviation Administration (FAA) Air Transportation Center of Excellence Cooperative Agreement 12-C-GA-ISU for the Partnership to Enhance General Aviation Safety, Accessibility and Sustainability (PEGASAS). The authors would like to thank the current project Technical Monitor, Mr. Benjamin J. Mahaffay, and the former project Technical Monitors, Mr. Jeffrey S. Gagnon (interim), Mr. Donald Barbagallo, and Dr. Charles A. Ishee for their invaluable guidance on this study. The authors would like to express their sincere gratitude to Mr. Paul Kremer of Iowa State University, CCEE (Civil, Construction, and Environmental Engineering Department), for his extremely kind assistance with providing access to the laboratories, required trainings, and consultation in conducting the experiments. The authors immensely thank Mr. Robert F. Steffes, Iowa State University (ISU), CCEE, Portland cement concrete (PCC) Lab Manager for his significant assistance with the lab investigations. Special thanks are expressed to Zoltek for providing carbon microfiber. Although the FAA has sponsored this project, it neither endorses nor rejects the findings of this research. The presentation of this information is in the interest of invoking comments by the technical community on the results and conclusions of the research.

References

[1] A. Sassani, H. Ceylan, S. Kim, K. Gopalakrishnan, A. Arabzadeh, P.C. Taylor, Factorial study on electrically conductive concrete mix design for heated pavement systems, in: Transp. Res. Board 96th Annu. Meet. No. 17-05347, Washington DC, 2017.

[2] A. Arabzadeh, H. Ceylan, S. Kim, K. Gopalakrishnan, A. Sassani, S. Sundararajan, P.C. Taylor, Influence of deicing salts on the water-repellency of Portland cement concrete coated with polytetrafluoroethylene and polyetheretherketone, in: ASCE Int. Conf. Highw. Pavements Airf. Technol., Philadelphia, Pennsylvania, 2017.

[3] A. Arabzadeh, H. Ceylan, S. Kim, K. Gopalakrishnan, A. Sassani, Superhydrophobic coatings on asphalt concrete surfaces, Transp. Res. Rec. 2551 (2016). J. Transp. Res. Board. No.

[4] Y. Lai, Y. Liu, D. Ma, Automatically melting snow on airport cement concrete pavement with carbon fiber grille, Cold Reg. Sci. Technol. 103 (2014) 57–62.

[5] T. Yang, Z.J. Yang, M. Singla, G. Song, Q. Li, Experimental study on carbon fiber tape–based deicing technology, J. Cold Reg. Eng. 26 (2012) 55–70.

[6] H. Ceylan, K. Gopalakrishnan, S. Kim, W. Cord, Heated transportation infrastructure Systems : existing ande emerging technologies. Civil, Constr. Environ. Eng. Conf. Present. Proceedings.23, Iowa State University, 2014.

[7] S. Yehia, C.Y. Tuan, Thin conductive concrete overlay for bridge deck deicing and anti-icing, Transp. Res. Rec. 1698 (2000) 45–53. J. Transp. Res. Board.

[8] W. Shen, H. Ceylan, K. Gopalakrishnan, S. Kim, A. Nahvi, Sustainability Assessment of Alternative Snow-Removal Methods for Airport Apron Paved Surfaces, No. DOT/FAA/TC-17/34, 2017.

[9] S.M.K. Hossain, L. Fu, R. Lake, Field evaluation of the performance of alternative deicers for winter maintenance of transportation facilities, Can. J. Civ. Eng. 448 (2015) 437–448.

[10] L. Fu, R. Omer, S.M.K. Hossain, C. Jiang, Experimental study of snow-melting performance of salt for snow and ice control of parking lots, in: Transp. Res. Board 92nd Annu. Meet., No. 13-1507, Washington DC, 2013.

[11] A. Christopher, J.E. Strong, P.A. Mosher, Effect of deicing salts on metal and organic matter mobilization in roadside soils, Environ. Sci. Technol. 26 (1992) 703–709.

[12] M. Bäckström, S. Karlsson, L. Bäckman, L. Folkeson, B. Lind, Mobilisation of heavy metals by deicing salts in a roadside environment, Water Res. 38 (2004) 720–732.

[13] M.A. Cunningham, E. Snyder, D. Yonkin, M. Ross, T. Elsen, Accumulation of deicing salts in soils in an urban environment, Urban Ecosyst. 11 (2008) 17–31.

[14] D. Sanzo, S.J. Hecnar, Effects of road de-icing salt (NaCl) on larval wood frogs (Rana sylvatica), Environ. Pollut. 140 (2006) 247–256.

[15] I. Czerniawska-Kusza, G. Kusza, M. Duzyński, Effect of deicing salts on urban soils and health status of roadside trees in the Opole Region, Environ. Toxicol. 19 (2004) 296–301.

[16] J.R. Karraker, E. Nancy, James P. Gibbs, Vonesh, Impacts of road deicing salt on the demography of vernal pool-breeding Amphibians, Ecol. Appl. 18 (2016) 724–734.

[17] D.M. Ramakrishna, T. Viraraghavan, Environmental impact of chemical deicers – a review, Water. Air. Soil Pollut. 166 (2005) 49–63.

[18] W. Shen, H. Ceylan, K. Gopalakrishnan, S. Kim, P.C. Taylor, C.R. Rehmann, Life cycle assessment of heated apron pavement system operations, Transp. Res. D Transp. Environ. 48 (2016) 316–331.

[19] H. Wang, C. Thakkar, X. Chen, S. Murrel, Life-cycle assessment of airport pavement design alternatives for energy and environmental impacts, J. Clean. Prod. 133 (2016) 163–171.

[20] D. Sterpi, A. Angelotti, O. Habibzadeh-Bigdarvish, D. Jalili, Assessment of thermal behaviour of thermo-active diaphragm walls based on monitoring data, J. Rock Mech. Geotech. Eng. (2018).

[21] X. Shi, Y. Rew, E. Ivers, C.-S. Shon, E.M. Stenger, P. Park, Effects of thermally modified asphalt concrete on pavement temperature, Int. J. Pavement Eng. 20 (2019) 669–681.

[22] A. Arabzadeh, H. Ceylan, S. Kim, K. Gopalakrishnan, A. Sassani, Superhydrophobic coatings on asphalt concrete surfaces: toward smart solutions for winter pavement maintenance, Transp. Res. Rec. 2551 (2016). J. Transp. Res. Board.

[23] H. Ceylan, A. Arabzadeh, A. Sassani, S. Kim, K. Gopalakrishnan, Innovative nano-engineered asphalt concrete for ice and snow controls in pavement systems, in: 6th Eurasphalt &Eurobitume Congr., Prague, Czech Republic, 2016.

[24] A. Arabzadeh, H. Ceylan, S. Kim, K. Gopalakrishnan, A. Sassani, S. Sundararajan, P.C. Taylor, Superhydrophobic coatings on Portland cement concrete surfaces, Constr. Build. Mater. 141 (2017) 393–401.

[25] A. Arabzadeh, H. Ceylan, S. Kim, K. Gopalakrishnan, A. Sassani, Fabrication of polytetrafluoroethylene-coated asphalt concrete biomimetic surfaces: a nanomaterials-based pavement winter maintenance approach, in: Int. Conf. Transp. Dev. 2016 Proj. Pract. Prosper. - Proc. 2016 Int. Conf. Transp. Dev., 2016.

[26] C. Chang, M. Ho, G. Song, Y.-L. Mo, H. Li, A feasibility study of self-heating concrete utilizing carbon nanofiber heating elements, Smart Mater. Struct. 18 (2009) 127001.

[27] A. Arabzadeh, M.A. Notani, A. Kazemian Zadeh, A. Nahvi, A. Sassani, H. Ceylan, Electrically conductive asphalt concrete: an alternative for automating the winter maintenance operations of transportation infrastructure, Compos. B Eng. (2019).

[28] J. Gomis, O. Galao, V. Gomis, E. Zornoza, P. Garcés, Self-heating and deicing conductive cement. Experimental study and modeling, Constr. Build. Mater. 75 (2015) 442–449.

[29] C.Y. Tuan, Implementation of Conductive Concrete for Deicing, Omaha, NE, 2008.

[30] H. Xu, D. Wang, Y. Tan, J. Zhou, M. Oeser, Investigation of design alternatives for hydronic snow melting pavement systems in China, J. Clean. Prod. 170 (2018) 1413–1422.

[31] H. Wang, L. Liu, Z. Chen, Experimental investigation of hydronic snow melting process on the inclined pavement, Cold Reg. Sci. Technol. 63 (2010) 44–49.

[32] P. Pan, S. Wu, Y. Xiao, G. Liu, A review on hydronic asphalt pavement for energy harvesting and snow melting, Renew. Sustain. Energy Rev. 48 (2015) 624–634.

[33] C.Y. Tuan, Roca spur bridge: the implementation of an innovative deicing technology, J. Cold Reg. Eng. 22 (2008) 1–15.

[34] R. Maggenti, R. Carter, R. Meline, Development of conductive polyester concrete for bridge-deck cathodic protection and ice control, Transp. Res. Rec. (1996) 61–69. J. Transp. Res. Board.

[35] E. Heymsfield, A.B. Osweiler, R.P. Selvam, M. Kuss, Feasibility of Anti-icing Airfield Pavements Using Conductive Concrete and Renewable Solar Energy, Fayetteville, Arkansas, 2013.

[36] V. Piskunov, O. Volod'ko, A. Porhunov, Composite materials for building heated coverings for roads and runways of airdromes, Mech. Compos. Mater. 44 (2008) 215–220.

[37] Z. Hou, Z. Li, J. Wang, Electrical conductivity of the carbon fiber conductive concrete, J. Wuhan Univ. Technol. Sci. Ed. 22 (2007) 346–349.

[38] C. Chang, M. Ho, G. Song, Y.L. Mo, H. Li, Improvement of electrical conductivity in carbon fiber-concrete composites using self consolidating technology, in: Earth Sp. 2010 Eng. Sci. Constr. Oper. Challenging Environ. ASCE, 2010, pp. 3553–3558.

[39] O. Galao, L. Bañón, F.J. Baeza, J. Carmona, P. Garcés, Highly conductive carbon fiber reinforced concrete for icing prevention and curing, Materials (Basel) 9 (2016) 281.

[40] J.P. Won, C.K. Kim, S.J. Lee, J.H. Lee, R.W. Kim, Thermal characteristics of a conductive cement-based composite for a snow-melting heated pavement system, Compos. Struct. 118 (2014) 106–111.

[41] M. Sun, W. Ying, L. Bin, X. Zhang, Deicing cconcrete pavement containing carbon black/carbon fiber conductive lightweight concrete composites, in: ICTIS 2011 Multimodal Approach to Sustain. Transp. Syst. Dev. Information, Technol. Implement., 2011, pp. 662–668.

[42] W. Chen, P. Gao, Performances of electrically conductive concrete with layered stainless steel fibers, Sustain. Constr. Mater. (2012) 163–171.

[43] J. Wu, J. Liu, F. Yang, Three-phase composite conductive concrete for pavement deicing, Constr. Build. Mater. 75 (2015) 129–135.

[44] M. Hambach, H. Moller, T. Neumann, D. Volkmer, Carbon fibre reinforced cement-based composites as smart floor heating materials, Compos. B Eng. 90 (2016) 465–470.

[45] Y. Rew, X. Shi, K. Choi, P. Park, Structural design and lifecycle assessment of heated pavement using conductive asphalt, J. Infrastruct. Syst. 24 (2018).

[46] H. Abdulla, H. Ceylan, S. Kim, K. Gopalakrishnan, P.C. Taylor, Y. Turkan, System requirements for electrically conductive concrete heated pavements, Transp. Res. Rec. 2569 (2016) 70–79. J. Transp. Res. Board. No.

[47] A. Bozorgzad, Y. Kim, H. David Lee, Determining the optimum content and stirring time of emerging dry polymer for asphalt using rotational viscometer, dynamic shear rheometer, and atomic force microscopy, Adv. Civil Eng. Mater. 7 (2018) 20170077.

[48] M. Arabani, S.M. Mirabdolazimi, A.R. Sasani, The effect of waste tire thread mesh on the dynamic behaviour of asphalt mixtures, Constr. Build. Mater. 24 (2010).

[49] S. Reubush, Effects of Storage on the Linear Viscoelastic Response of Polymer-Modified Asphalt at Intermediate to High Temperatures, Diss. Virginia Polytech. Inst. State Univ., 1999.

[50] M. Notani, Mohammad Ali Mokhtarnejad, Investigating the rheological and self-healing capability of toner-modified asphalt binder, Proc. Inst. Civil Eng. Mater. (2018) 1–9.

[51] M.A. Notani, F. Moghadas Nejad, A. Khodaii, P. Hajikarimi, Evaluating fatigue resistance of toner-modified asphalt binders using the linear amplitude sweep test, Road Mater. Pavement Des. (2018) 1–14.

[52] A. Arabzadeh, H. Ceylan, S. Kim, K. Gopalakrishnan, A. Sassani, S. Sundararajan, P.C. Taylor, Superhydrophobic coatings on Portland cement concrete surfaces, Constr. Build. Mater. 141 (2017).

[53] V. Hejazi, K. Sobolev, M. Nosonovsky, From superhydrophobicity to icephobicity: forces and interaction analysis, Sci. Rep. 3 (2013) 2194.

[54] I. Flores-vivian, V. Hejazi, M.I. Kozhukhova, M. Nosonovsky, K. Sobolev, Self-assembling particle-siloxane coatings for superhydrophobic concrete, ACS Appl. Mater. Interfaces 5 (2013) 13284–13294.

[55] M. Nosonovsky, K. Sobolev, Superhydrophobic and Icephobic concrete and Construction Materials, 2013, pp. 85–92.

[56] M. Horgnies, J.J. Chen, Superhydrophobic concrete surfaces with integrated microtexture, Cement Concr. Compos. 52 (2014) 81–90.

[57] J.H.O. Nascimento, P. Pereira, E. Freitas, F. Fernandes, Development and characterization of a superhydrophobic and anti-ice asphaltic nanostructured material for road pavements, in: 7th Int. Conf. Maintenace Rehabil. Pavements Technol. Control, Auckland, New Zealand, 2012.

[58] J. Orlikowski, S. Cebulski, K. Darowicki, Electrochemical investigations of conductive coatings applied as anodes in cathodic protection of reinforced concrete, Cement Concr. Compos. 26 (2004) 721–728.

[59] J. Xu, W. Yao, Electrochemical studies on the performance of conductive overlay material in cathodic protection of reinforced concrete, Constr. Build. Mater. 25 (2011) 2655–2662.

[60] A. Cañón, P. Garcés, M.A. Climent, J. Carmona, E. Zornoza, Feasibility of electrochemical chloride extraction from structural reinforced concrete using a sprayed conductive graphite powder-cement paste as anode, Corros. Sci. 77 (2013) 128–134.

[61] P.C. Ma, N.A. Siddiqui, G. Marom, J.K. Kim, Dispersion and functionalization of carbon nanotubes for polymer-based nanocomposites: a review, Compos. Part A Appl. Sci. Manuf. 41 (2010) 1345–1367.

[62] J.E. Mates, I.S. Bayer, J.M. Palumbo, P.J. Carroll, C.M. Megaridis, Extremely stretchable and conductive water-repellent coatings for low-cost ultra-flexible electronics, Nat. Commun. 6 (2015) 1–8.

[63] J.E. Mates, I.S. Bayer, M. Salerno, P.J. Carroll, Z. Jiang, L. Liu, C.M. Megaridis, Durable and flexible graphene composites based on artists' paint for conductive paper applications, Carbon N. Y. 87 (2015) 163–174.

[64] H. Chu, Z. Zhang, Y. Liu, J. Leng, Silver particles modified carbon nanotube paper/glassfiber reinforced polymer composite material for high temperature infrared stealth camouflage, Carbon N. Y. 98 (2016) 557–566.

[65] B.O. Lee, W.J. Woo, H.S. Park, H.S. Hahm, J.P. Wu, M.S. Kim, Influence of aspect ratio and skin effect on EMI shielding of coating materials fabricated with carbon nano ber/PVDF, Carbon 7 (2008) 1839–1843.

[66] L. Liu, A. Das, C.M. Megaridis, Terahertz shielding of carbon nanomaterials and their composites - a review and applications, Carbon 69 (2014) 1–16.

[67] A. Das, H.T. Hayvaci, M.K. Tiwari, I.S. Bayer, D. Erricolo, C.M. Megaridis, Superhydrophobic and conductive carbon nanofiber/PTFE composite coatings for EMI shielding, J. Colloid Interface Sci. 353 (2011) 311–315.

[68] P. Slobodian, P. Riha, R. Benlikaya, P. Svoboda, D. Petras, A flexible multifunctional sensor based on carbon nanotube/polyurethane composite, IEEE Sens. J. 13 (2013) 4045–4048.

[69] P. Slobodian, P. Riha, P. Saha, A highly-deformable composite composed of an entangled network of electrically-conductive carbon-nanotubes embedded in elastic polyurethane, Carbon N. Y. 50 (2012) 3446–3453.

[70] J.M. Engel, J. Chen, D. Bullen, C. Liu, Polyurethane rubber as a MEMS material: characterization and demonstration of an all-polymer two-axis artificial hair cell flow sensor, in: 18th IEEE Int. Conf. Micro Electro Mech. Syst. 2005, 2005, pp. 279–282.

[71] S. Laflamme, I. Pinto, H. Saleem, M. Elkashef, K. Wang, Conductive paint-filled cement paste sensor for accelerated percolation, in: Struct. Heal. Monit. Insp. Adv. Mater. Aerospace, Civ. Infrastruct., 2015, pp. 1–8.

[72] E. Andreoli, K.S. Liao, A. Cricini, X. Zhang, R. Soffiatti, H.J. Byrne, S.A. Curran, Carbon black instead of multiwall carbon nanotubes for achieving comparable high electrical conductivities in polyurethane-based coatings, Thin Solid Films 550 (2014) 558–563.

[73] J. Engel, J. Chen, N. Chen, S. Pandya, C. Liu, Multi-Walled carbon nanotube filled conductive elastomers: materials and application to micro transducersa, in: IEEE MEMS, 2006, pp. 246–249.

[74] C.Y. Lee, J.H. Bae, T.Y. Kim, S.H. Chang, S.Y. Kim, Using silane-functionalized graphene oxides for enhancing the interfacial bonding strength of carbon/epoxy composites, Compos. Part A Appl. Sci. Manuf. 75 (2015) 11–17.

[75] C. Su, J. Li, H. Geng, Q. Wang, Q. Chen, Fabrication of an optically transparent super-hydrophobic surface via embedding nano-silica, Appl. Surf. Sci. 253 (2006) 2633–2636.

[76] M.K. Tiwari, I.S. Bayer, G.M. Jursich, T.M. Schutzius, C.M. Megaridis, Highly liquid-repellent, large-area, nanostructured poly(vinylidene fluoride)/poly(ethyl

2-cyanoacrylate) composite coatings: particle filler effects, ACS Appl. Mater. Interfaces. 2 (2010) 1114–1119.
[77] I.S. Bayer, M.K. Tiwari, C.M. Megaridis, Biocompatible poly(vinylidene fluoride)/cyanoacrylate composite coatings with tunable hydrophobicity and bonding strength, Appl. Phys. Lett. 93 (2008) 1–4.
[78] A. Nahvi, M. Kazem Sadoughi, A. Arabzadeh, A. Sassani, C. Hu, H. Ceylan, S. Kim, Multi-objective bayesian optimization of super hydrophobic coatings on asphalt concrete surfaces, J. Comput. Des. Eng. (2018).
[79] N. Vourdas, A. Tserepi, E. Gogolides, Nanotextured super-hydrophobic transparent poly(methyl methacrylate) surfaces using high-density plasma processing, Nanotechnology 18 (2007) 125304.
[80] J. Lin, J. Zhu, D.R. Swanson, L. Milco, Cross-linking and physical characteristics of a water-based nonstick hydrophobic coating, Langmuir 7463 (1996) 6676–6680.
[81] L.D. Poulikakos, C. Papadaskalopoulou, B. Hofko, F. Gschösser, A. Cannone Falchetto, M. Bueno, M. Arraigada, J. Sousa, R. Ruiz, C. Petit, M. Loizidou, M.N. Partl, Harvesting the unexplored potential of European waste materials for road construction, Resour. Conserv. Recycl. 116 (2017) 32–44.
[82] C. Gao, Y.Z. Jin, H. Kong, R.L.D. Whitby, S.F. a Acquah, G.Y. Chen, H. Qian, A. Hartschuh, S.R.P. Silva, S. Henley, P. Fearon, H.W. Kroto, D.R.M. Walton, Polyurea-functionalized multiwalled carbon nanotubes: synthesis, morphology, and Raman spectroscopy, J. Phys. Chem. B. 109 (2005) 11925–11932.
[83] H.C. Kuan, C.C.M. Ma, W.P. Chang, S.M. Yuen, H.H. Wu, T.M. Lee, Synthesis, thermal, mechanical and rheological properties of multiwall carbon nanotube/waterborne polyurethane nanocomposite, Compos. Sci. Technol. 65 (2005) 1703–1710.
[84] S. Rana, N. Karak, J.W. Cho, Y.H. Kim, Enhanced dispersion of carbon nanotubes in hyperbranched polyurethane and properties of nanocomposites, Nanotechnology 19 (2008).
[85] J. Ryszkowska, M. Jurczyk-Kowalska, T. Szymborski, K.J. Kurzydłowski, Dispersion of carbon nanotubes in polyurethane matrix, Phys. E Low-Dimens. Syst. Nanostruct. 39 (2007) 124–127.
[86] D.K. Chattopadhyay, K.V.S.N. Raju, Structural engineering of polyurethane coatings for high performance applications, Prog. Polym. Sci. 32 (2007) 352–418.
[87] K. Golovin, M. Boban, J.M. Mabry, A. Tuteja, Designing self-healing superhydrophobic surfaces with exceptional mechanical durability, ACS Appl. Mater. Interfaces. 9 (2017) 11212–11223.
[88] M.H. Irfan, Polyurethanes in the construction industry, in: Chem. Technol. Thermosetting Polym. Constr. Appl., 1998, pp. 123–144.
[89] P. Duarte, J.R. Correia, J.G. Ferreira, F. Nunes, M.R.T. Arruda, Experimental and numerical study on the effect of repairing reinforced concrete cracked beams strengthened with carbon fibre reinforced polymer laminates, Can. J. Civ. Eng. 41 (2014) 222–231.
[90] A. Sassani, H. Ceylan, S. Kim, A. Arabzadeh, P.C. Taylor, K. Gopalakrishnan, Development of carbon fiber-modified electrically conductive concrete for implementation in des moines international airport, Case Stud. Constr. Mater. 8 (2018) 277–291.
[91] P.-W. Chen, D.D.L. Chung, Concrete as a new strain/stress sensor, Compos. B Eng. 27B (1996) 11–23.
[92] D.D.L. Chung, Cement reinforced with short carbon fibers : a multifunctional material, Compos. B Eng. 31 (2000) 511–526.
[93] J.M.L. Reis, R.P. Lima, S.D. Vidal, Effect of rate and temperature on the mechanical properties of epoxy BADGE reinforced with carbon nanotubes, Compos. Struct. (2018) 89–94.
[94] G.M. Kim, B.J. Yang, G.U. Ryu, H.K. Lee, The electrically conductive carbon nanotube (CNT)/cement composites for accelerated curing and thermal cracking reduction, Compos. Struct. 158 (2016) 20–29.
[95] G.M. Kim, B.J. Yang, K.J. Cho, E.M. Kim, H.K. Lee, Influences of CNT dispersion and pore characteristics on the electrical performance of cementitious composites, Compos. Struct. 164 (2017) 32–42.
[96] G.M. Kim, F. Naeem, H.K. Kim, H.K. Lee, Heating and heat-dependent mechanical characteristics of CNT-embedded cementitious composites, Compos. Struct. 136 (2016) 162–170.
[97] R.N. Howser, H.B. Dhonde, Y.L. Mo, Self-sensing of carbon nanofiber concrete columns subjected to reversed cyclic loading, Smart Mater. Struct. 20 (2011).
[98] Y. He, L. Lu, S. Jin, S. Hu, Conductive aggregate prepared using graphite and clay and its use in conductive mortar, Constr. Build. Mater. 53 (2014) 131–137.
[99] J.M. Balbus, A.D. Maynard, V.L. Colvin, V. Castranova, G.P. Daston, R.A. Denison, K.L. Dreher, P.L. Goering, A.M. Goldberg, K.M. Kulinowski, N.A. Monteiro-Riviere, G. Oberdörster, G.S. Omenn, K.E. Pinkerton, K.S. Ramos, K.M. Rest, J.B. Sass, E.K. Silbergeld, B.A. Wong, Meeting report: hazard assessment for nanoparticles-report from an interdisciplinary workshop, Environ. Health Perspect. 115 (2007) 1654–1659.
[100] X. Gong, L. Liu, Y. Liu, J. Leng, An electrical-heating and self-sensing shape memory polymer composite incorporated with carbon fiber felt, Smart Mater. Struct. 25 (2016).
[101] A. Ameli, P.U. Jung, C.B. Park, Electrical properties and electromagnetic interference shielding effectiveness of polypropylene/carbon fiber composite foams, Carbon N. Y. 60 (2013) 379–391.
[102] A. Nahvi, V.D. Pyrialakou, P. Anand, S.M.S. Sadati, K. Gkritza, H. Ceylan, K. Cetin, A. Arabzzadeh, S. Kim, K. Gopalakrishnan, P.C. Taylor, Integrated stochastic life cycle benefit cost analysis of hydronically-heated apron pavement system, J. Clean. Prod. (2019).
[103] A. Nahvi, S.M.S. Sadati, K. Cetin, H. Ceylan, A. Sassani, S. Kim, Towards resilient infrastructure systems for winter weather events: integrated stochastic economic evaluation of electrically conductive heated airfield pavements, Sustain. Cities Soc. 41 (2018) 195–204.
[104] O. Habibzadeh-Bigdarvish, X. Yu, G. Lei, T. Li, A.J. Puppala, Life-Cycle cost-benefit analysis of Bridge deck de-icing using geothermal heat pump system: a case study of North Texas, Sustain. Cities Soc. 47 (2019) 101492.
[105] D.D. Chung, Dispersion of short fibers in cement, J. Mater. Civ. Eng. 17 (2005) 379–383.
[106] J. Xiong, Z. Zheng, X. Qin, M. Li, H. Li, X. Wang, The thermal and mechanical properties of a polyurethane/multi-walled carbon nanotube composite, Carbon N. Y. 44 (2006) 2701–2707.
[107] S. Haseebuddin, K.V.S.N. Raju, D. Krishna, P.J. Reddy, M. Yaseen, Temperature dependence of viscosity of polyurethane polyol solutions: application of rheological models, J. Appl. Polym. Sci. 59 (1996) 29–36.
[108] S. Velankar, S.L. Cooper, Microphase separation and rheological properties of polyurethane melts. 3. Effect of block incompatibility on the viscoelastic properties, Macromolecules 33 (2000) 395–403.
[109] N. Xie, X. Shi, D. Feng, B. Kuang, H. Li, Percolation backbone structure analysis in electrically conductive carbon fiber reinforced cement composites, Compos. B Eng. 43 (2012) 3270–3275.
[110] S. Wu, L. Mo, Z. Shui, Z. Chen, Investigation of the conductivity of asphalt concrete containing conductive fillers, Carbon N. Y. 43 (2005) 1358–1363.
[111] P. Cong, P. Xu, S. Chen, Effects of carbon black on the anti aging, rheological and conductive properties of SBS/asphalt/carbon black composites, Constr. Build. Mater. 52 (2014) 306–313.
[112] A. Sassani, H. Ceylan, S. Kim, K. Gopalakrishnan, A. Arabzadeh, P.C. Taylor, Influence of mix design variables on engineering properties of carbon fiber-modified electrically conductive concrete, Constr. Build. Mater. 152 (2017) 168–181.
[113] S. Wen, D.D.L. Chung, The role of electronic and ionic conduction in the electrical conductivity of carbon fiber reinforced cement, Carbon N. Y. 44 (2006) 2130–2138.
[114] T.S. Light, S.L. Licht, Conductivity and resistivity of water from the melting to critical points, Anal. Chem. 59 (1987) 2327–2330.
[115] A. Arabzadeh, H. Ceylan, S. Kim, A. Sassani, K. Gopalakrishnan, M. Mina, Electrically-conductive asphalt mastic: temperature dependence and heating efficiency, Mater. Des. 157 (2018) 303–313.
[116] N. Hawkins, O. Smadi, S. Knickerbocker, A. Pike, P. Carlson, Evaluating All-Weather Pavement Markings in illinois : Volume 1, Research Report No. FHWA-ICT-15-018, Ames, Iowa, USA, 2015.
[117] ASTM, ASTM E303-93, Standard Test Method for Measuring Surface Frictional Properties Using the British Pendulum Tester, 2013, pp. 1–5.
[118] H. Kim, Y. Seo, C. Hyun, A hybrid conceptual cost estimating model for large building projects, Autom. ConStruct. 25 (2012) 72–81.
[119] S. An, U. Park, K. Kang, M. Cho, H. Cho, Application of support vector machines in Assessing Conceptual Cost Estimates, J. Comput. Civil Eng. 21 (2007) 259–264.
[120] C.C. Chen, Y.C. Chou, Electrical-conductivity fluctuations near the percolation threshold, Phys. Rev. Lett. 54 (1985) 2529–2532.
[121] G. Wu, J. Lin, Q. Zheng, M. Zhang, Correlation between percolation behavior of electricity and viscoelasticity for graphite filled high density polyethylene, Polymer (Guildf) 47 (2006) 2442–2447.
[122] W.L. Song, M.S. Cao, M.M. Lu, J. Liu, J. Yuan, L.Z. Fan, Improved dielectric properties and highly efficient and broadened bandwidth electromagnetic attenuation of thickness-decreased carbon nanosheet/wax composites, J. Mater. Chem. C. 1 (2013) 1846–1854.
[123] Y. Chekanov, R. Ohnogi, S. Asai, M. Sumita, Positive temperature coefficient effect of epoxy resin filled with short carbon fibers, Polym. J. 30 (1998) 381–387.
[124] S. Paschen, M.N. Bussac, L. Zuppiroli, E. Minder, B. Hilti, Tunnel junctions in a polymer composite, J. Appl. Phys. 78 (1995) 3230–3237.
[125] W.S. Bao, S.A. Meguid, Z.H. Zhu, G.J. Weng, Tunneling resistance and its effect on the electrical conductivity of carbon nanotube nanocomposites, J. Appl. Phys. 111 (2012).
[126] N. Reininger, Building Construction Costs with RSMeans Data, 76th Annua, The Gordian Group, 2018.
[127] A. Arabzadeh, M.A. Notani, A.K. Zadeh, A. Nahvi, A. Sassani, H. Ceylan, Electrically conductive asphalt concrete: an alternative for automating the winter maintenance operations of transportation infrastructure, Compos. B Eng. (2019) 106985.
[128] P. Anand, A. Nahvi, H. Ceylan, D. Pyrialakou, K. Gkritza, S. Kim, P.C. Taylor, Energy and Financial Viability of Hydronic Heated Pavement Systems, 2017.